Supporting Information

Achieving Ultrahigh Charge-Discharge Efficiency and Energy Storage in High-Temperature Polar Polymeric Dielectrics via Restrained Dipole Interactions

Baotieliang Wang, Jiawei Zou, Bo Liu, Zhaoyang Wang, Bei Li, Donghua Xu, Qi Li,* Shifang Luan**

B. Wang, J. Zou, Z. Wang, D. Xu, S. Luan
State Key Laboratory of Polymer Physics and Chemistry, Changchun Institute of Applied Chemistry, Chinese Academy of Sciences, Changchun 130022, China
B. Wang, S. Luan
School of Applied Chemistry and Engineering, University of Science and Technology of China, Hefei 230026, China
Q. Li
State Key Laboratory of Power System, Department of Electrical Engineering, Tsinghua University, Beijing 100084, China
B. Liu, B. Li
School of Materials Science and Engineering, Research Center for Materials Genome Engineering, Wuhan University of Technology, Wuhan 430070, China
Corresponding Author:
jwzou@ciac.ac.cn; qili1020@tsinghua.edu.cn; sfluan@ciac.ac.cn.

Experimental Procedures

Preparation: m-Phenylenediamine was sourced from Merck Sigma-Aldrich, and 2-methylsulfonylethanol was acquired from Shanghai Aladdin Biochemical Technology Co., Ltd. Other monomers, 3-Hydroxypropionitrile, 3,5-Dinitrobenzoyl chloride and 4,4'-(Hexafluoroisopropylidene)Diphthalic Anhydride (6FDA) used in the preparation of PI-N and PI-S, the catalyzer Pyridine, Triethylamine as well as the solvent 1-Methyl-2-Pyrrolidinone (NMP) which were all purchased from Energy Chemical Co., Ltd.

The mixture of diamine 2-Cyanoethyl 3,5-Diaminobenzoate and m-Phenylenediamine with different content ratios, along with the dianhydride of 6FDA was dissolved in NMP in a 1:1 ratio, stirred at room temperature for 12 h to yield a viscous and uniform poly (amic acid) solution. 10 times the molar amount of Pyridine and 3 times the molar amount of Acetic Anhydride were added into the solution and stirred continuously for 16 h. The reaction PI solvent was precipitated by adding to excess cold methanol, purified 5 times, and then collected by filtration and dried under 60 °C in a vacuum. The evenly mixed solution of N_{100}, N_{75}, N_{50}, N_{25} and N_0 were in strict accordance with the distribution of the molar ratio of the two diamines: 100:0, 75:25, 50:50, 25:75, 0:100. The subsequent preparation process of PI-S copolymer films is the same as that of the PI-N, while the diamine monomer was 2-(Methylsulfonyl)ethyl 3,5-Diaminobenzoate. The PI-derived polymers were dissolved in NMP and the solution was cast on flat, clean glass. The mass solvent was removed at 100 °C for 2 h, and the

polymer film was finally dried at 200 °C in a vacuum oven for 10 h to form the dielectric film with a thickness of about 10 μm.

Characterization: The ^{1}H-NMR spectra of correlative compounds were recorded on a Bruker AVANCE III 500 MHz spectrometer. The Fourier infrared spectroscopy (FT-IR) curves were measured on a Bruker alpha. The M_n and PDI of the polyimide synthesized in this study were measured by Agilent PL-GPC 220 with DMF as the mobile phase. Thermal gravimetric analyzer (TGA) curves were carried out on a Mettler Toledo TGA2 with a heating rate of 10 °C/min under a nitrogen atmosphere. Dynamic thermal analysis (DMA) was recorded on TA DMA Q800, the tested film thickness was about 50 μm. XRD tests were performed using Brucker D8 ADVANCE. with measuring angle from 5° to 70°, equipped with a Cu K_α source (λ = 1.54 Å). The valence band X-ray photoelectron spectroscopy (VB-XPS) tests were measured on Thermo ESCALAB 250XI. Dielectric properties were performed through an Agilent LCR instrument (4294A). The high-field polarization-electric field (P-E) loops were obtained by PolyK (PK CPE20B) using a modified Sawyer-Tower circuit, in which the dielectric films were exposed to a triangular unipolar wave at a frequency of 100 Hz. Dielectric breakdown strength was recorded on a Trek 610C at a voltage rise rate of 500 V s^{-1}. The experiment was conducted in a silicone oil bath to reduce surface corona discharge. The leakage currents, direct current conductivity, and TSDC profiles were

evaluated using an electrometer (Keithley 6517A). The leakage current was collected with an electric field gradient of 25 MV m^{-1}. The TSDC characterization procedures are as follows: after a 30-minute polarization at 200 °C and rapid cooling to -10 °C for 5 minutes, the specimens were short-circuited, and the current was recorded as the temperature increased from -10 to 250 °C with the heating rate of 5 °C min^{-1}. The amorphous cells were collected using Materials Studio (MS) software. Each of the amorphous cells consists of 5 molecular chains, with the polymerization of 12. Molecular dynamic simulations were conducted under isothermal (NVT) and isoenergetic equilibration (NVE) conditions and at least five annealing processes were performed on the amorphous cells of all polymers.

Density functional theory (DFT) calculation

DFT calculations were carried out using the Vienna ab initio Simulation Package (VASP). The electron exchange and correlation energy were treated within the generalized gradient approximation (GGA) in the Perdew-Burke-Ernzerhof functional (PBE). And the calculations were done with a plane-wave basis set defined by a cut-off energy of 500 eV. The energy calculation and geometry optimization were finished when the electronic energy tolerance reached 1×10^{5} eV/atom and the maximum component of the force on any atom as smaller than 0.02 eV/Å, respectively.

To consider the van der Waals interaction, the empirical correction in the Grimme

scheme (DFT-D3) was adopted. And the charge density difference was visualized using VESTA. The Gaussian16 package was employed to optimize the geometric structure of different polymer molecules at the B3LYP/6-31G* level of theory in vacuum. The independent gradient models based on Hirshfeld partition (IGMH) analyses were carried out using the software Multiwfn to study the weak interaction between polar nitrile groups and were visualized using VMD.

The charge density difference integrated over the *xy* plane is defined as

$$\Delta\rho = \iint_{-\infty}^{+\infty} (\rho_{PI/Efield} - \rho_{PI}) dxdy \quad (1)$$

Where ρ_{PI}, $\rho_{PI/Efield}$ are the charge density of PI, and it in external electric field of 0.001 eV/Å, respectively. The charge displacement curve is calculated by integrating $\Delta\rho$ along the *z* axis:

$$\Delta Q = \int_{-\infty}^{z} \Delta\rho dz \quad (2)$$

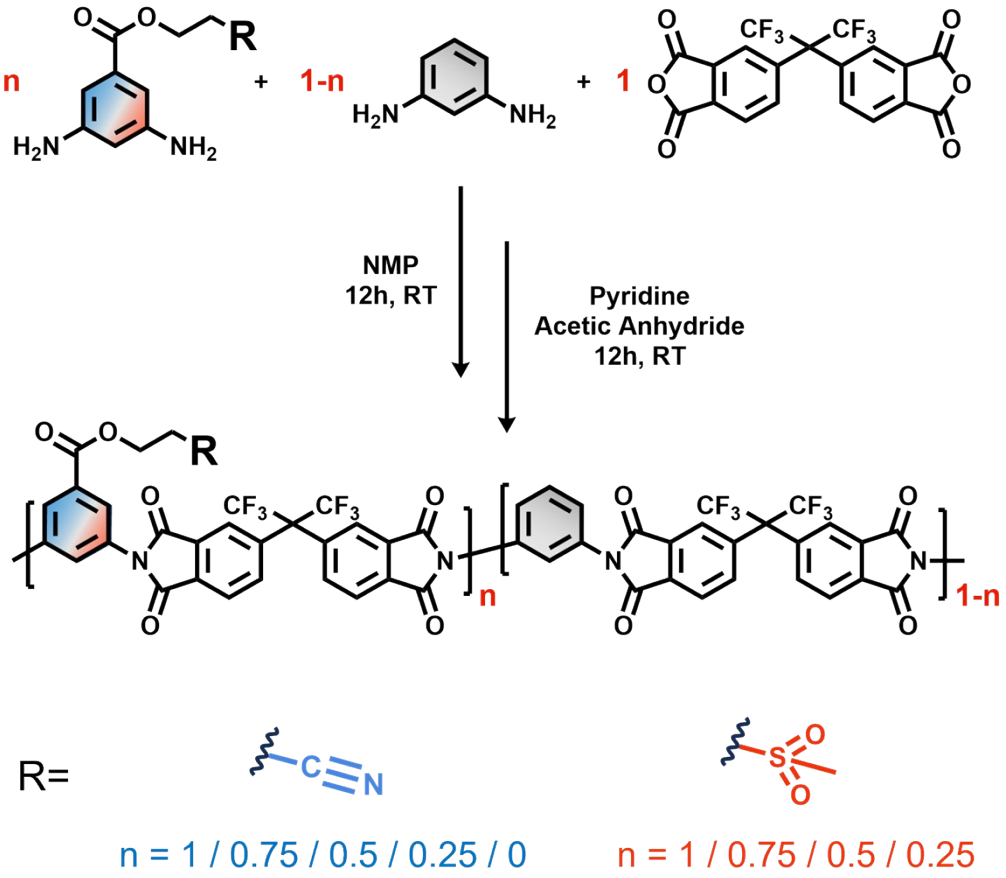

Figure S1. Structures and synthesis routes of polyimides with polar groups nitrile & sulfone.

Synthesis of diamine monomers DNB-CN and DNB-SO_2.

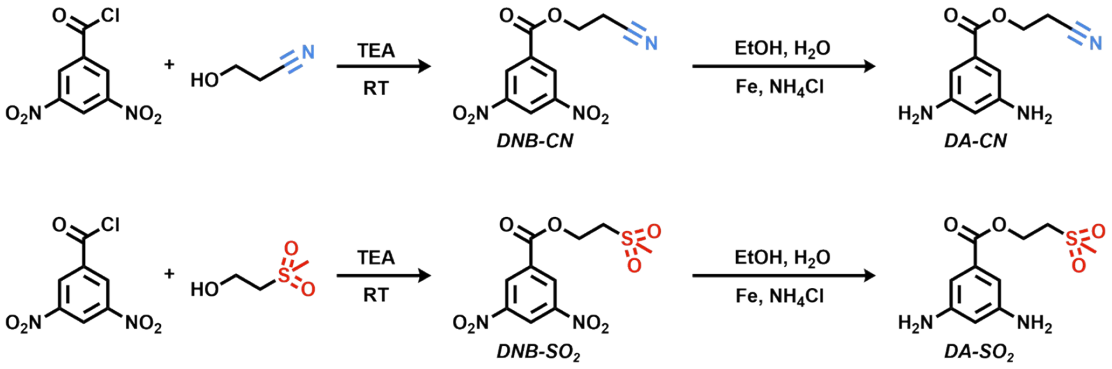

Figure S2. Synthetic routes of diamine monomer.

The synthesis routes of DNB-CN and DNB-SO_2 followed a similar procedure. First, a 500 mL three-neck round-bottom flask was immersed in an ice-water bath, and 20 mmol of 3-hydroxypropionitrile for DNB-CN (or 3-(methylsulfonyl)propan-1-ol for DNB-SO_2) along with 30 mmol of TEA (4.17 ml) were added to the flask. Subsequently, 200 mL of anhydrous THF was introduced. Then, a mixture of 3,5-dinitrobenzoyl chloride (24 mmol, 2.59 g) and a small quantity of THF was slowly introduced into the flask under vigorous magnetic stirring. The reaction was conducted for 10 hours at 0 ˚C under atmospheric conditions. The resulting reaction solution was then subjected to three consecutive extractions with water to obtain the organic phase. The product was subsequently purified using chromatography on silica gel, employing dichloromethane as the eluent. Finally, the solvent was removed under reduced pressure, and faint yellow powder was obtained with a yield of about 75%.

Synthesis of DA-CN and DA-SO_2.

Dinitrobenzene monomers with polar side groups were reduced to form diamine compounds DA-CN and DA-SO_2. At first, prepare a 250 mL three-neck flask equipped with Fe (160 mmol, 8.96 g) and NH_4Cl (80 mmol, 4.28 g), the mixture of water (30 mL), ethanol (90 mL) containing the precursor dinitrobenzene (20 mmol) was then added to the flask. The reaction mixture was heated at 80 ˚C under mechanical stirring conditions and reflux for 12 hours. Then the mixture was filtered and remove the solvent of filtrate. Dissolve dried product powder into acetonitrile and remove insoluble residues, the product was further purified by chromatography on neutral alumina, employing a mixture of acetonitrile/dichloromethane as eluent, and finally yellow solid was gained with a yield of 85%.

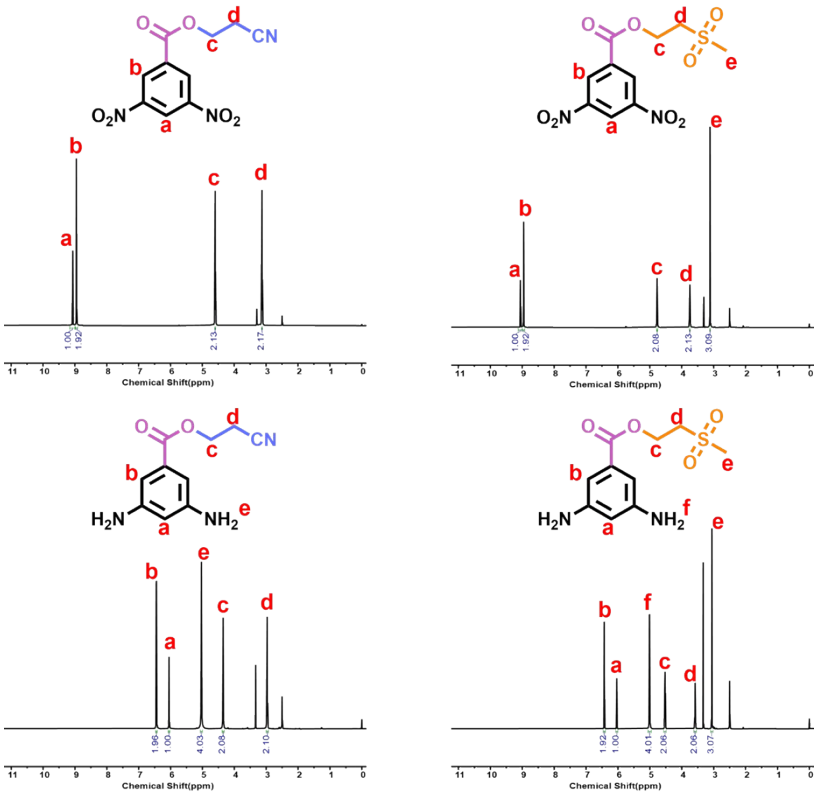

Figure S3. ^{1}H-NMR (500 MHz, DMSO-d_6) spectrum of monomer DNB-CN, DNB-SO_2, DA-CN and DA-SO_2.

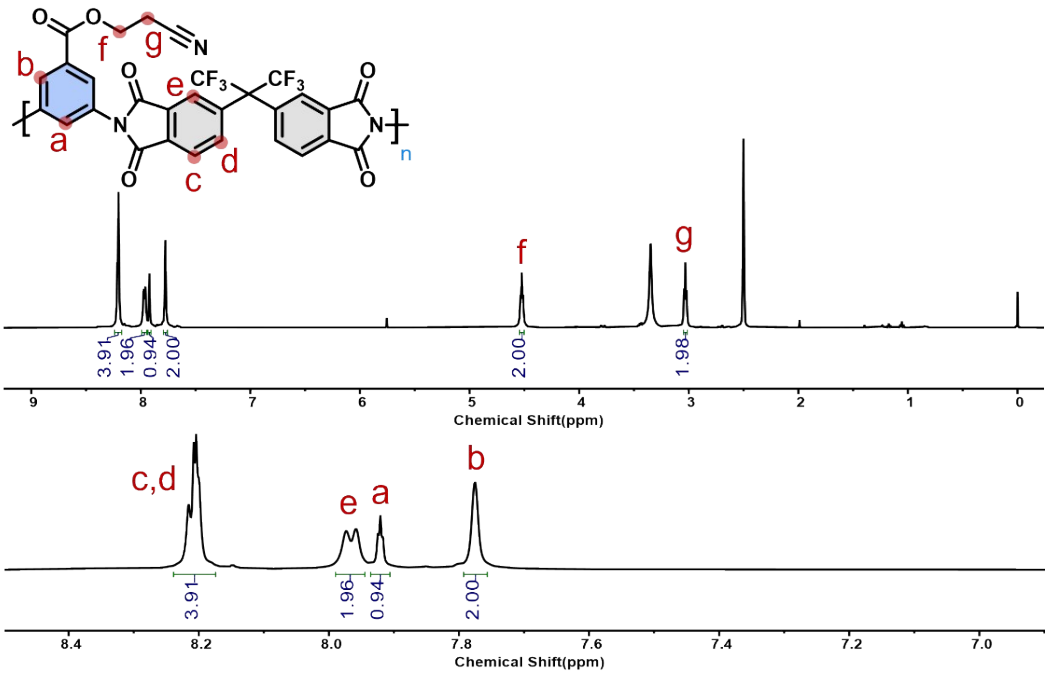

Figure S4. ^{1}H-NMR (500 MHz, DMSO-d_6) of N_{100}.

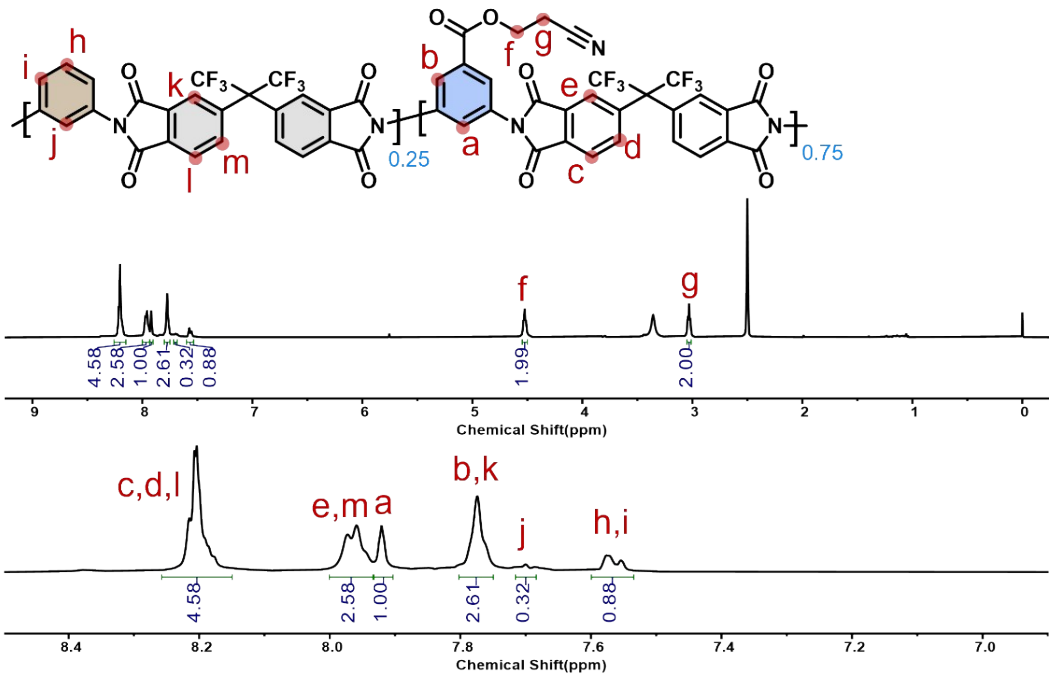

Figure S5. ^{1}H-NMR (500 MHz, DMSO-d_6) of N_{75}. The copolymerization ratio of the repeating unit where the nitrile group is located can be inferred from the integration ratio of characteristic peaks “a” and “j”, which is 1.00/ (1.00+0.32) = **75.7%**.

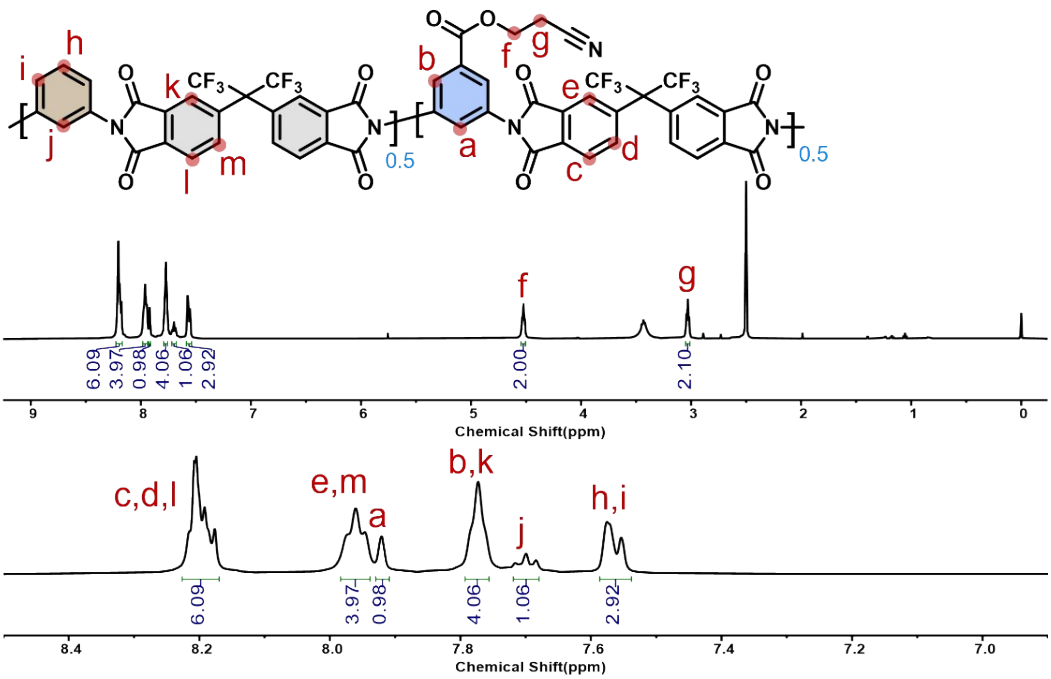

Figure S6. ^{1}H-NMR (500 MHz, DMSO-d_6) of N_{50}. The copolymerization ratio of the repeating unit where the nitrile group is located can be inferred from the integration ratio of characteristic peaks “a” and “j”, which is 1.00/ (1.00+1.06) = **48.5%**.

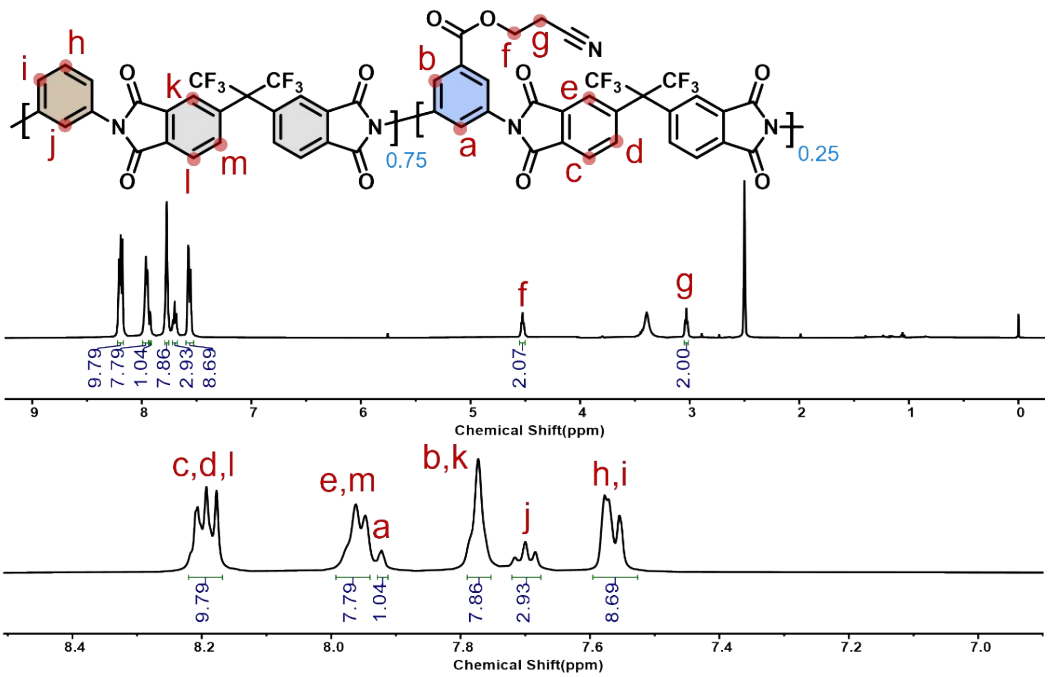

Figure S7. ^{1}H-NMR (500 MHz, DMSO-d_6) of N_{25}. The copolymerization ratio of the repeating unit where the nitrile group is located can be inferred from the integration ratio of characteristic peaks “a” and “j”, which is 1.04/ (1.04+2.93) = **25.4%**.

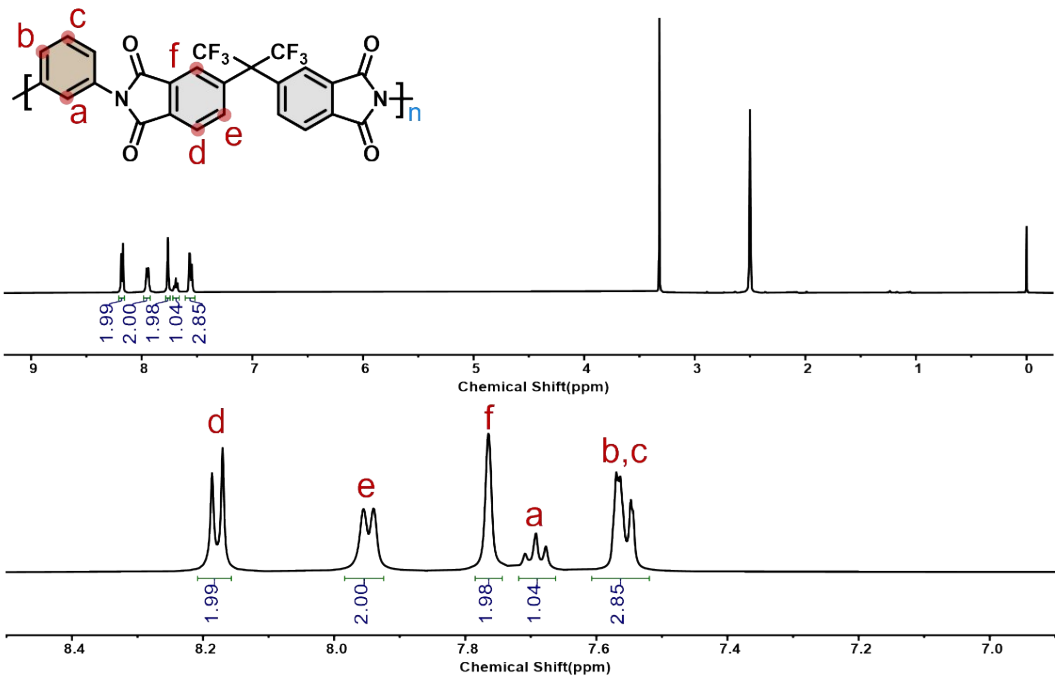

Figure S8. ^{1}H-NMR (500 MHz, DMSO-d_6) of N_0.

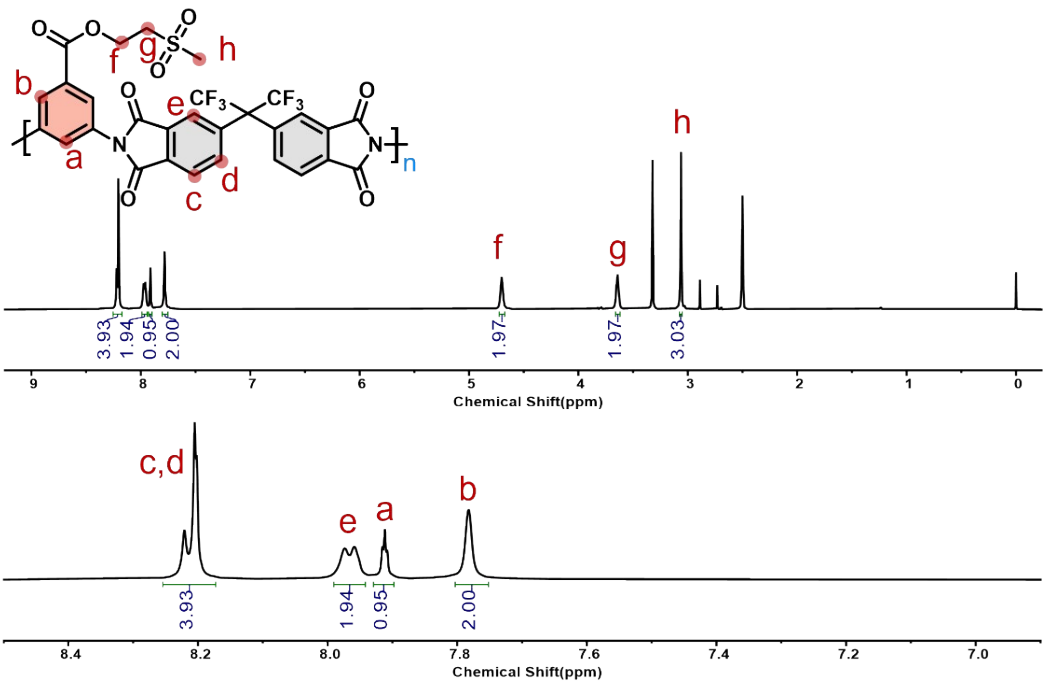

Figure S9. ^{1}H-NMR (500 MHz, DMSO-d_6) of S_{100}.

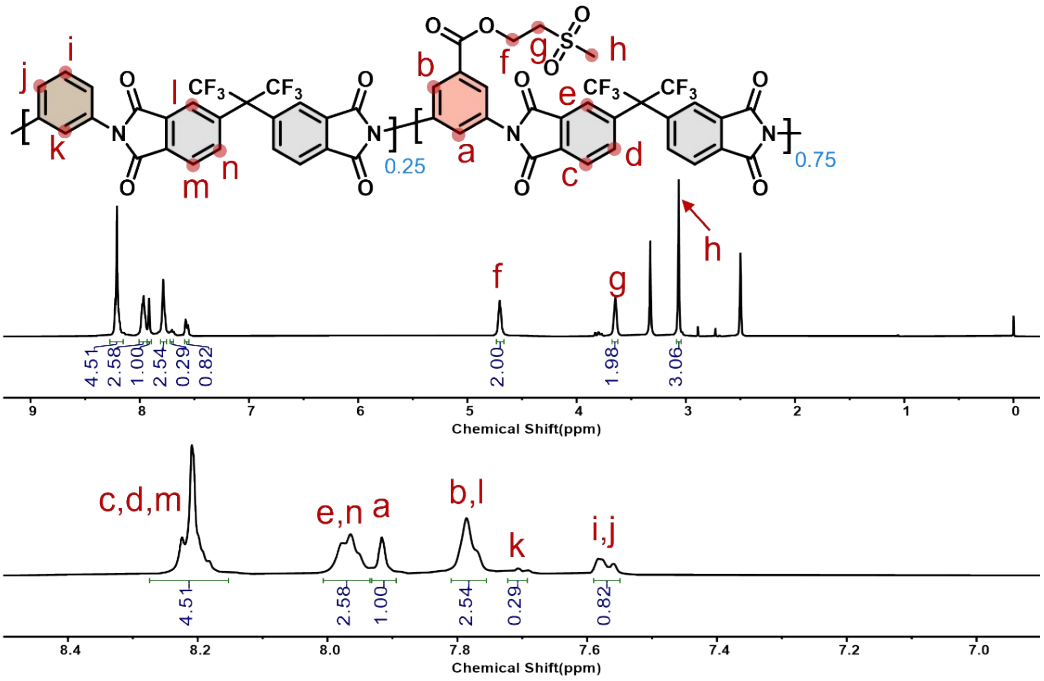

Figure S10. ^{1}H-NMR (500 MHz, DMSO-d_6) of S_{75}. The copolymerization ratio of the repeating unit where the sulfone group is located can be inferred from the integration ratio of characteristic peaks “a” and “k”, which is 1.00/ (1.00+0.29) = **77.5%**.

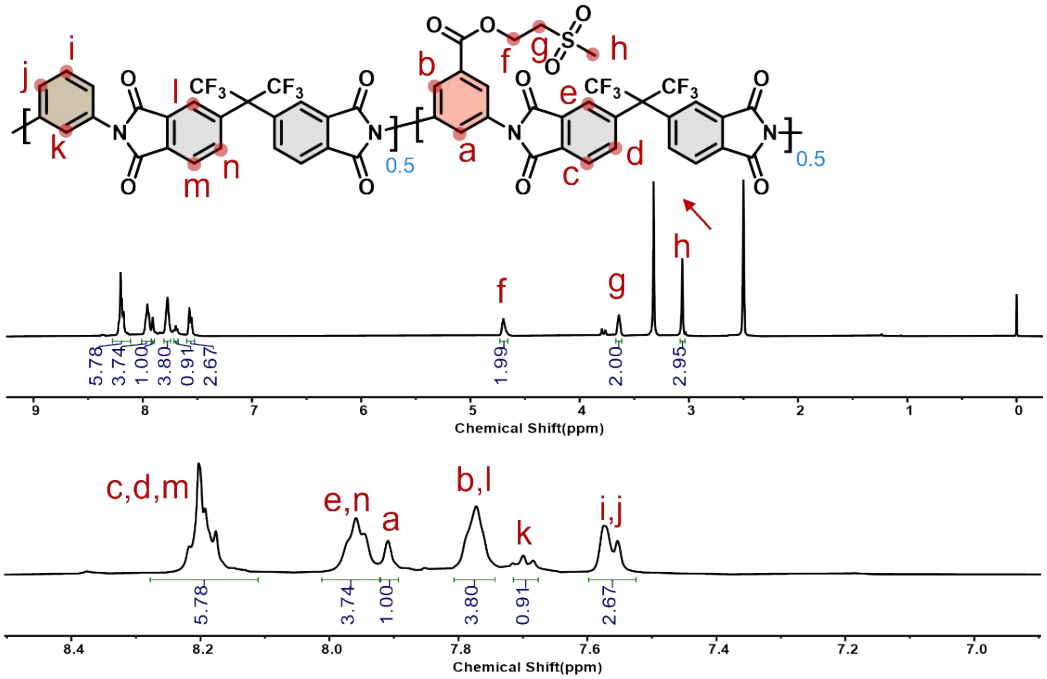

Figure S11. ^{1}H-NMR (500 MHz, DMSO-d_6) of S_{50}. The copolymerization ratio of the repeating unit where the sulfone group is located can be inferred from the integration ratio of characteristic peaks “a” and “k”, which is 1.00/ (1.00+0.91) = **52.3%**.

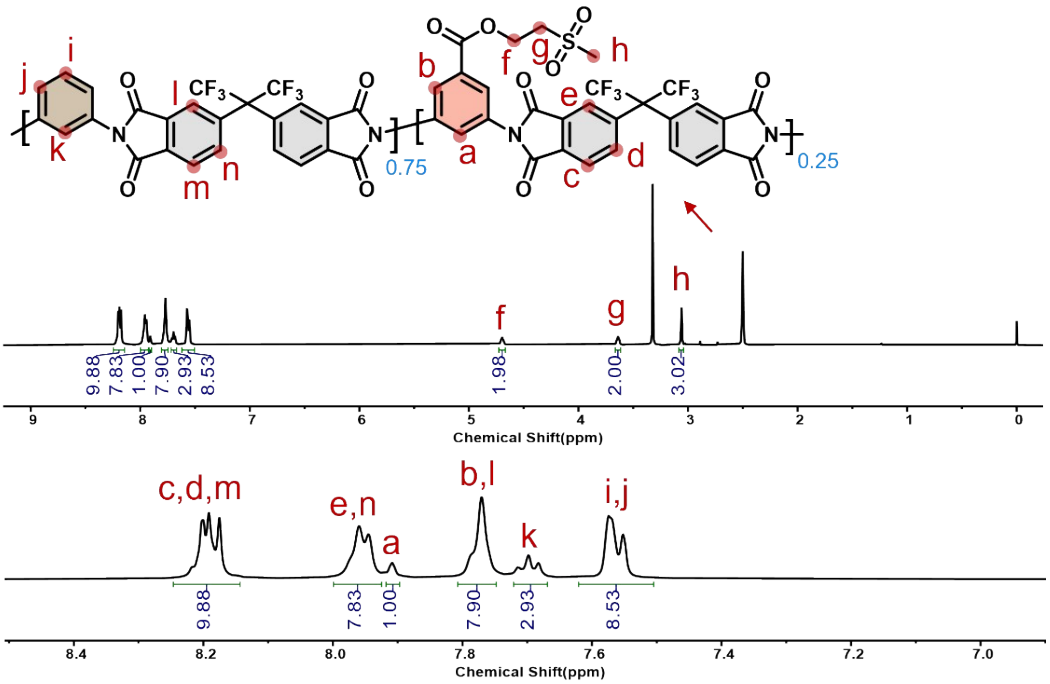

Figure S12. ^{1}H-NMR (500 MHz, DMSO-d_6) of S_{25}. The copolymerization ratio of the repeating unit where the sulfone group is located can be inferred from the integration ratio of characteristic peaks “a” and “k”, which is 1.00/ (1.00+2.93) = **25.4%**.

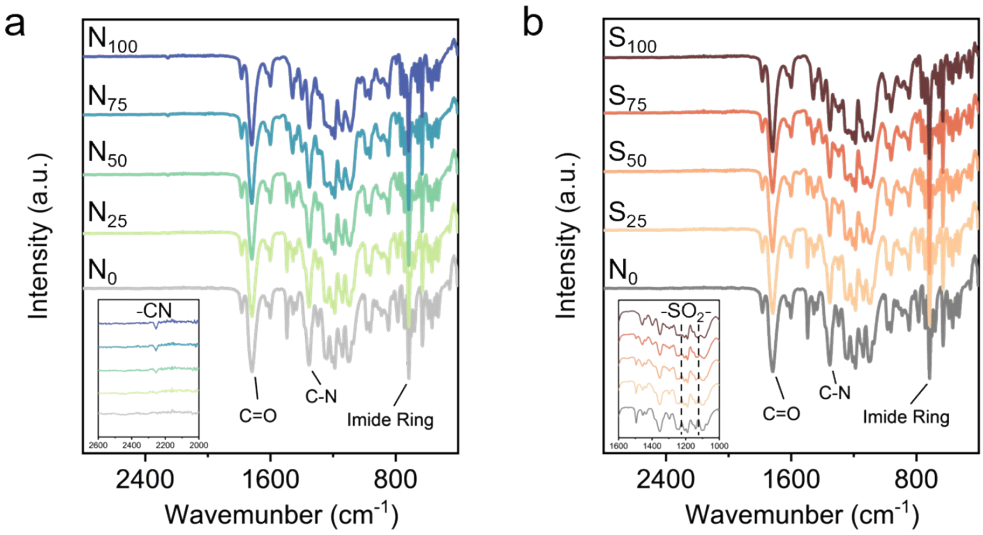

Figure S13. ATR-FTIR spectra of polymers containing -CN and -SO_2-. In the infrared spectra, the peaks such as the stretching absorption of C=O (1720−1785 cm^{-1}), C−N stretch (~1360 cm^{-1}), and imide ring (~725 cm^{-1}) exist in both PI-derived polymers. The peaks around 2250 cm^{-1} are from nitrile groups. Peaks at 1220 cm^{-1} and 1120 cm^{-1} are attributed to the sulfone groups.

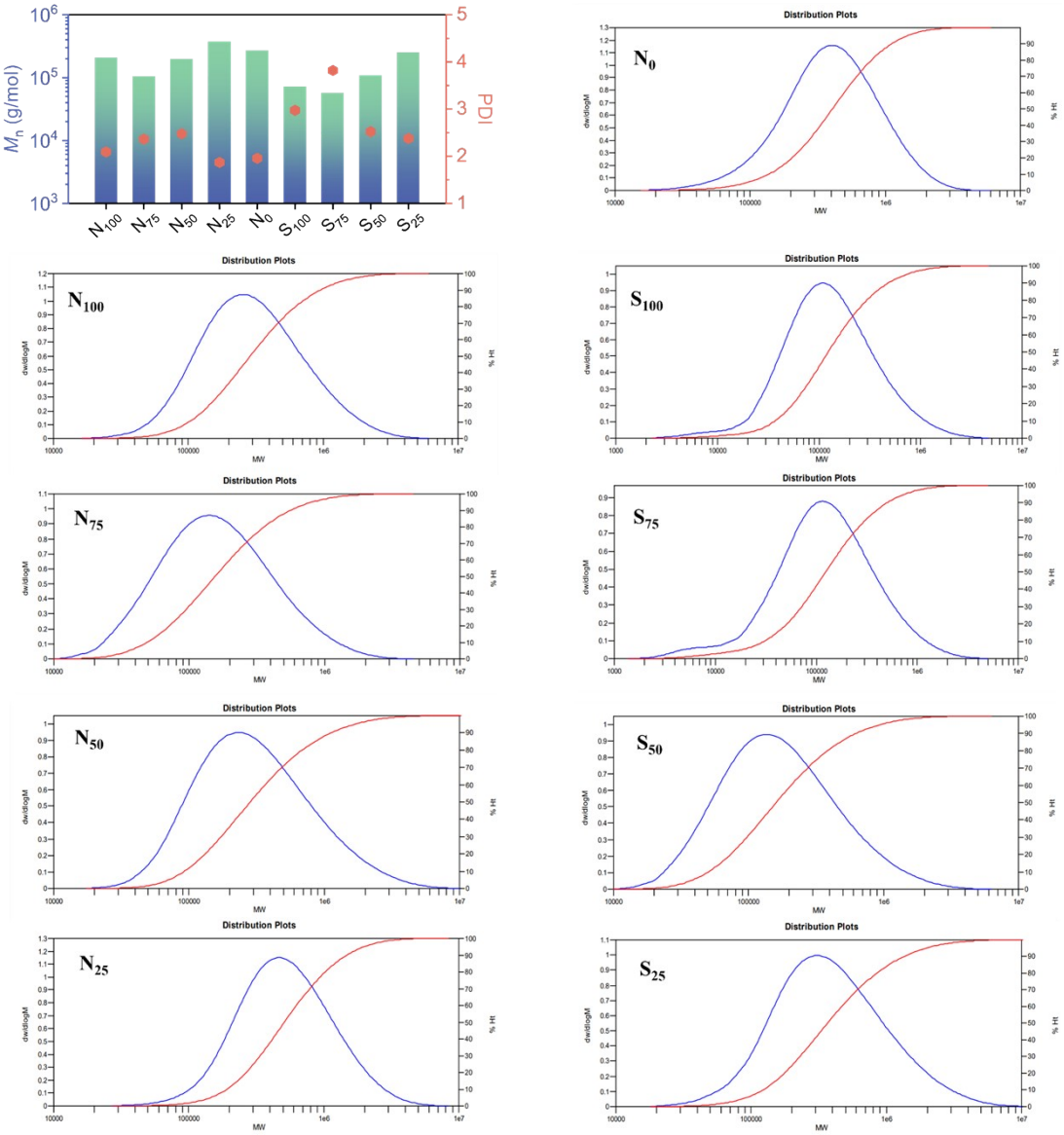

Figure S14. M_n and PDI values of PI-derived polymers characterized by GPC with N, N-Dimethylformamide (DMF) as the mobile phase.

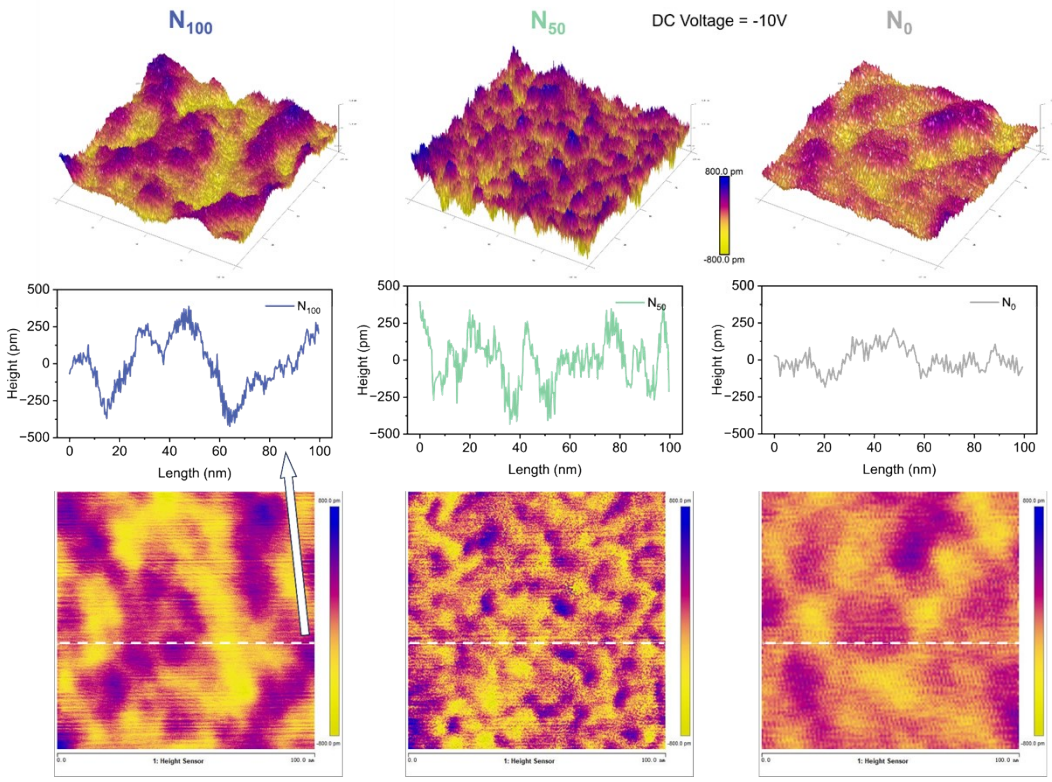

Figure S15. 3D and 2D images of the aggregation states of N_{100}, N_{50} and N_0 under 10 V bias voltage.

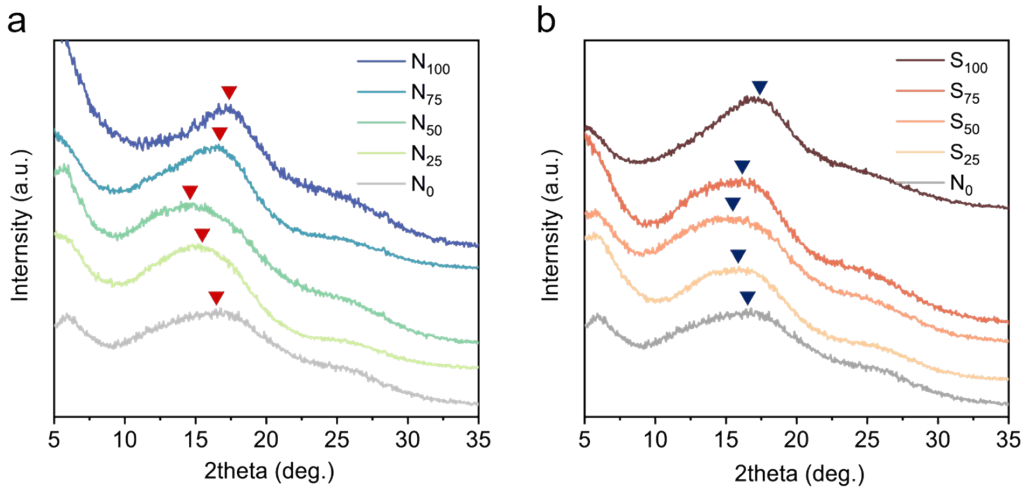

Figure S16. XRD spectra of polymers. N_{100} and S_{100} exhibit the smallest interchain spacing and the sharpest diffraction peak.

The molecular chain distances for N_0, N_{50}, and N_{100} are measured at 5.43 Å, 6.11 Å, and 5.23 Å, respectively, indicating an initial increase followed by a decrease. We attribute this trend to two main factors: first, the steric hindrance caused by the bulky side chains tends to increase the interchain distance; while in the case of N_{50}, the dipole interactions among the polar groups remain relatively weak, which allows for an increase in the distance between chains. However, as the dipole density rises, the excessive dipole interactions can lead to the attraction of polar groups, resulting in structural changes within the molecular chains. Consequently, in N_{75} and N_{100}, the increase in dipole interactions surpasses the steric hindrance effect, leading to a reduction in chain distance. This conclusion could also applies to N_0, S_{50} and S_{100}.

Table S1. Interchain spacing of polar polymers

Sample	N_0	N_{25}	N_{50}	N_{75}	N_{100}	S_{25}	S_{50}	S_{75}	S_{100}
2θ (deg.)	16.31	15.10	14.47	16.22	16.93	15.75	15.22	16.02	16.90
d-spacing(Å)	5.43	5.86	6.11	5.45	5.23	5.62	5.81	5.52	5.24

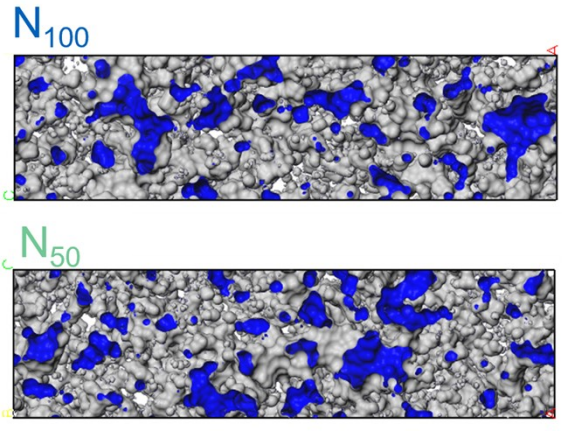

Figure S17. Molecular dynamic simulations of N_{100} and N_{50}, N_{50} have the bigger free volume ratio, and thus a smaller chain entanglement density and larger chain relative distance.

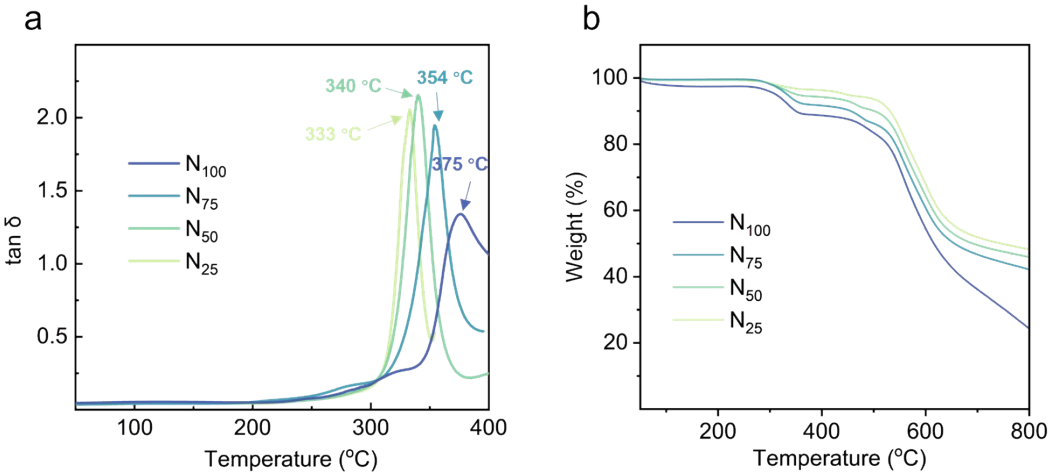

Figure S18. a) Dynamic Mechanical Analysis curves of nitrile polymers and b) Thermal gravimetric Analysis curves of nitrile polyimides. No tan δ peaks corresponding to the T_g were observed before the decomposition temperature of 300 °C.

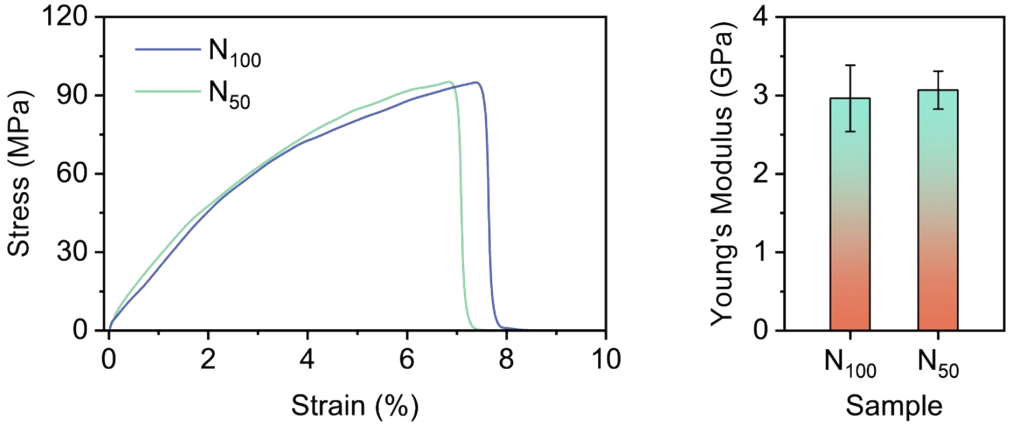

Figure S19. Stress-strain curves and average Young's modulus of N_{100} and N_{50}.

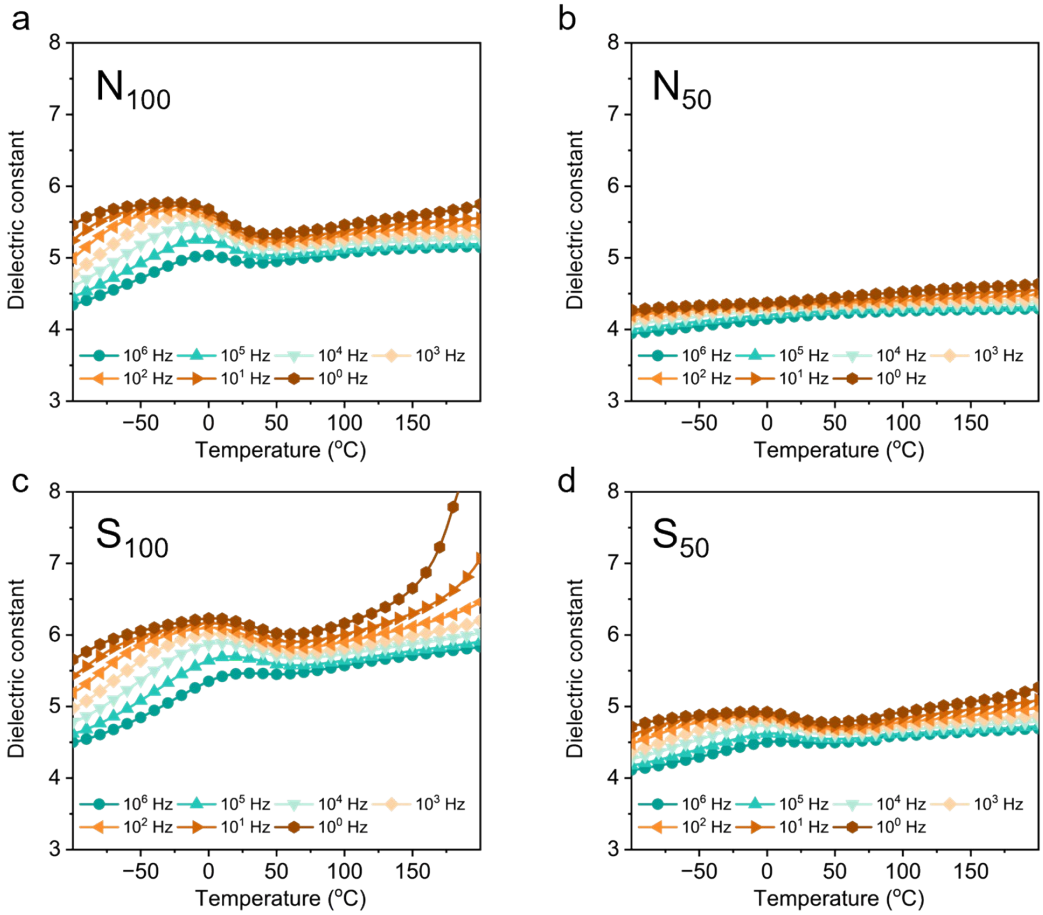

Figure S20. Temperature-dependence BDS permittivity curves of a) N_{100}, b) N_{50}, c) S_{100} and d) S_{50}. The sub-T_g transition around 0 °C was not observed in N_{50}, indicating the decoupled side groups, only the permittivity values decreased from the higher polar group content to the lower. However, in S_{50}, the dipoles are still coupled, because the positions of the sub-T_g peak have not changed significantly compared to S_{100}.

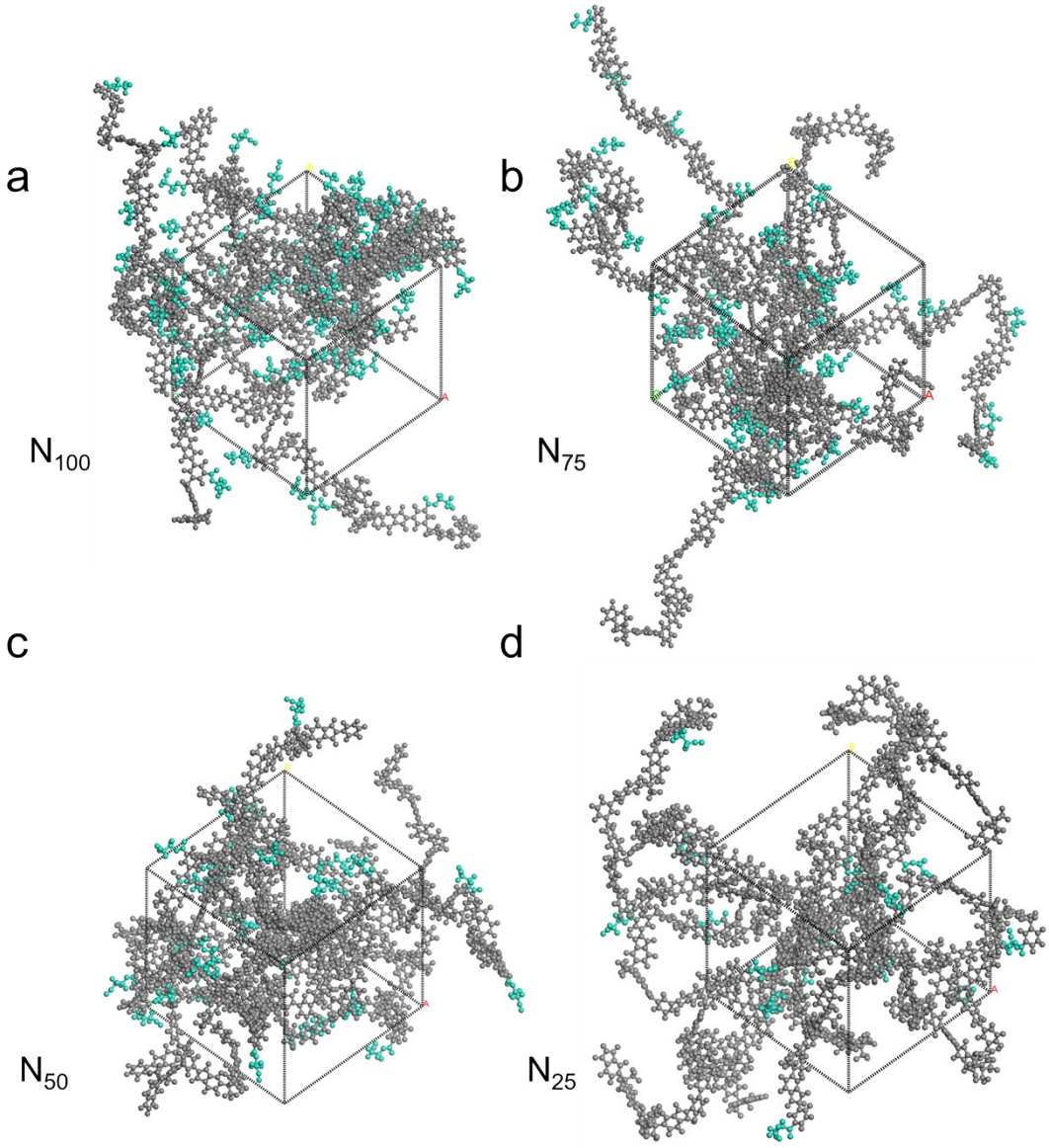

Figure S21. Amorphous cells of nitrile polymers, with relatively decoupled polar groups at low contents.

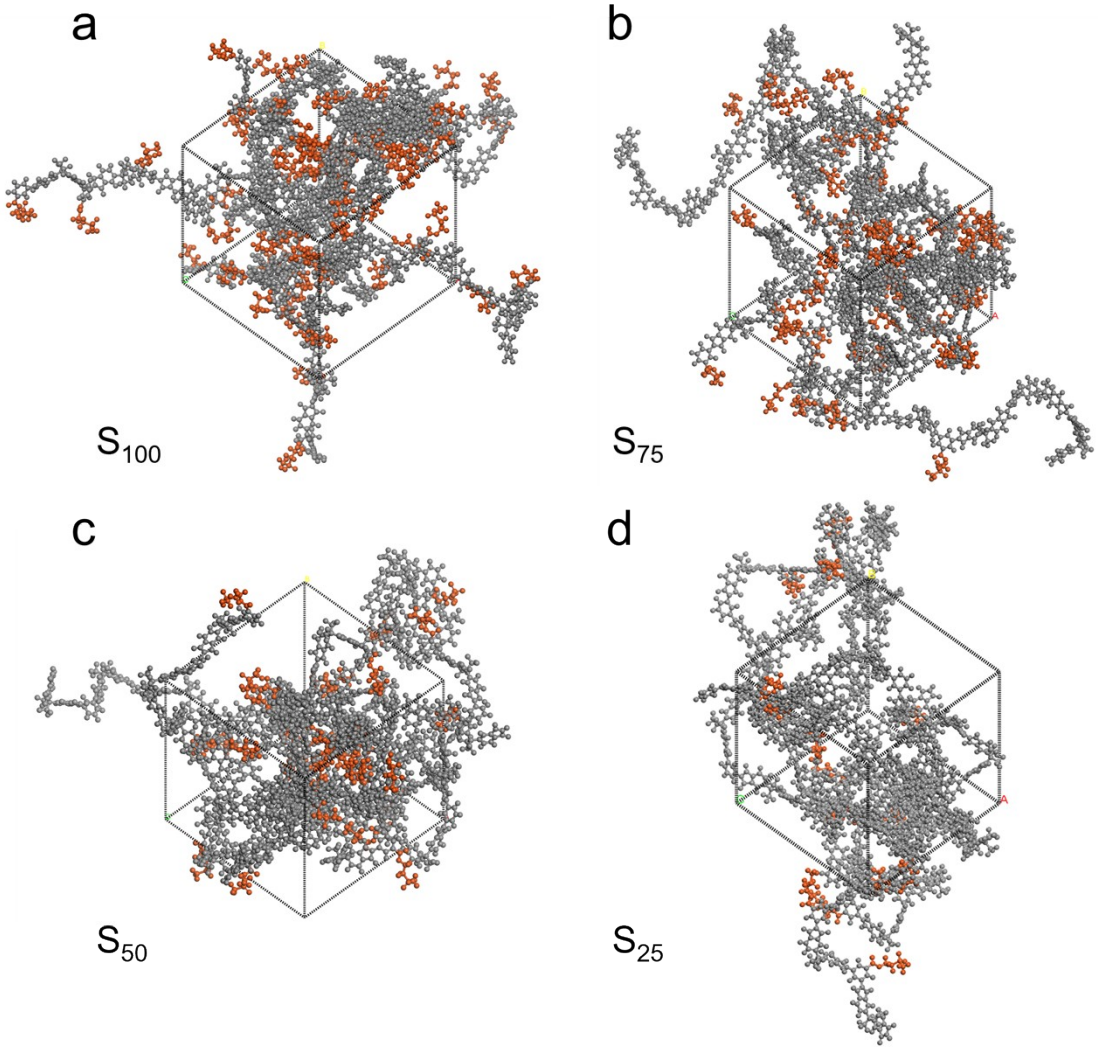

Figure S22. Amorphous cells of sulfone polymers. The dipoles (marked in orange) were more aggregated than those of nitrile polymers.

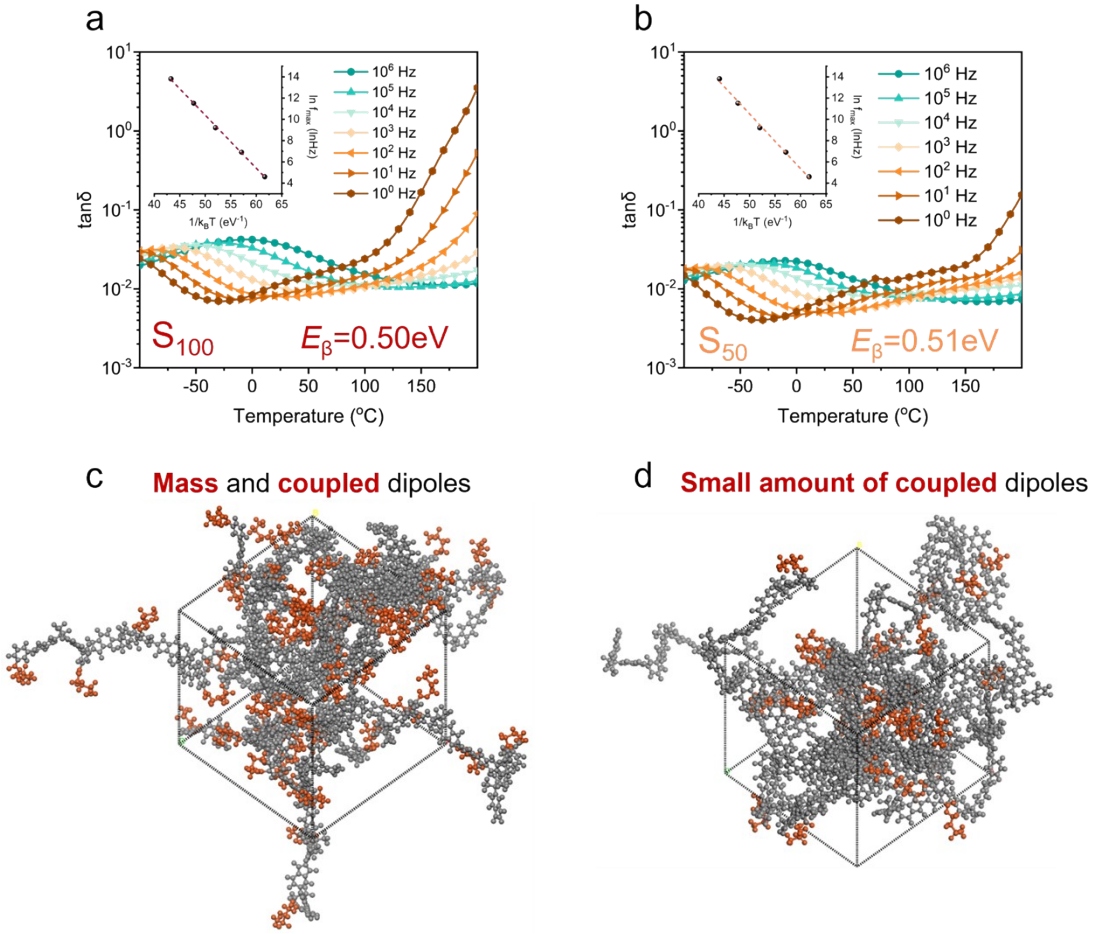

Figure S23. Temperature scanning BDS tan δ spectra of a) S_{100} and b) S_{50}. Polymer amorphous cells of c) S_{100} and d) S_{50}. The tan δ diminished with the decreased sulfone group content. However, the β transition peaks ranging from -100 to 0 °C exist in both sulfone polymers, and the calculated $E_β$ for S_{100} and S_{50} are 0.50 eV and 0.51 eV, respectively. Indicated that the mobility of sulfone groups was not enhanced by decreasing distribution from 100% to 50% probably because of their stronger dipole interactions, the lower tan δ is just attributed to the less sulfone contents, which could also be observed in simulation results.

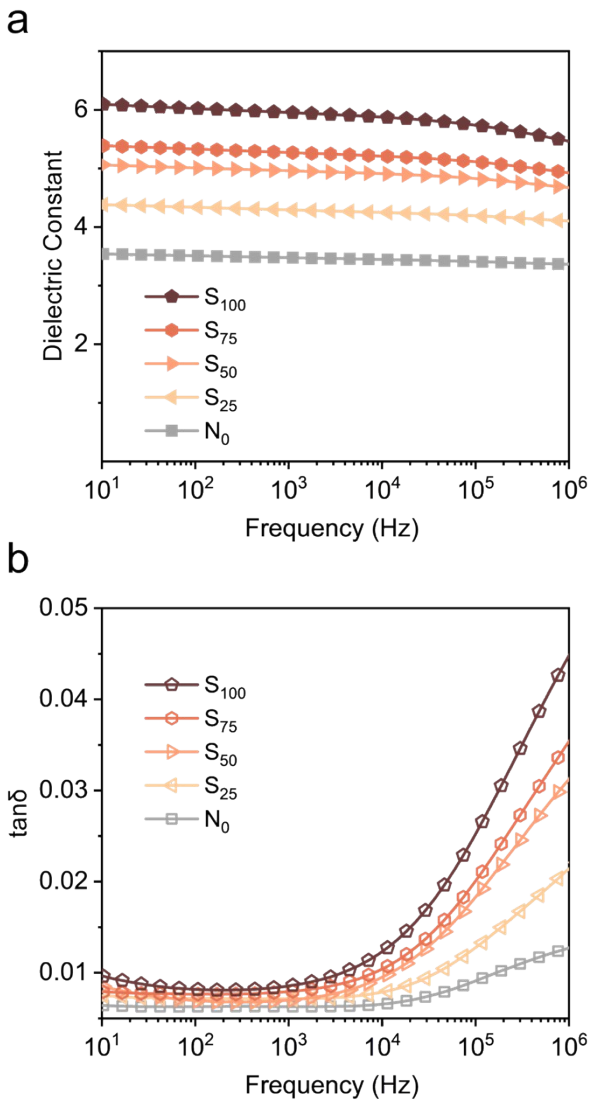

Figure S24. Dielectric performances of sulfone polymers at room temperature. Both permittivity and tan δ are positively correlated with the content of polar groups. Besides, the S_{25} exhibits the obvious decrease of tan δ at a higher frequency, possibly due to its partly decoupled sulfone group structure.

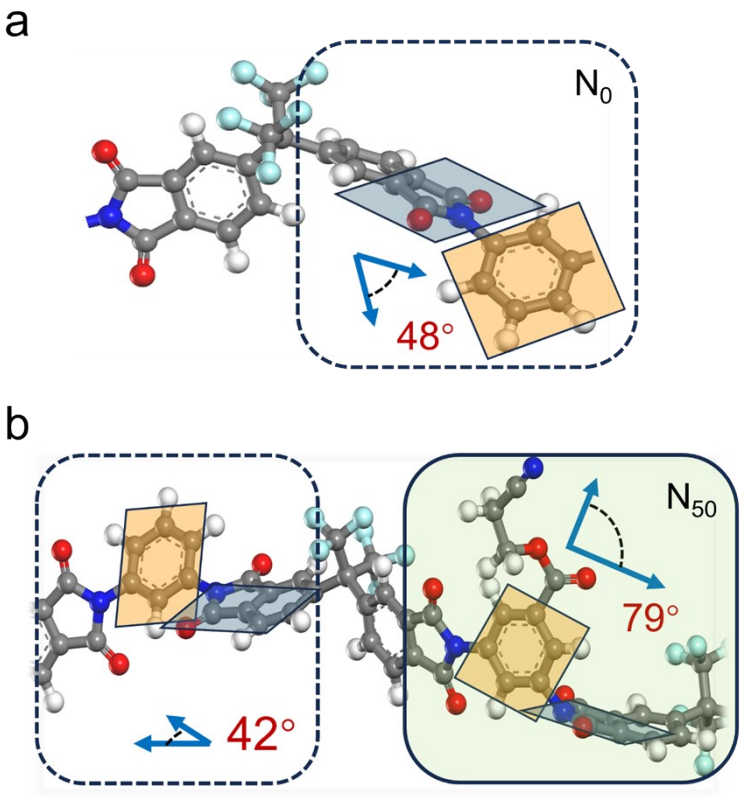

Figure S25. Dihedral angles between the adjacent conjugation planes of polymers repeat units with or without polar groups, larger dihedral angles are beneficial for improving the insulation performance of PI-derived polymers with E_g >3.3 eV at high temperature.

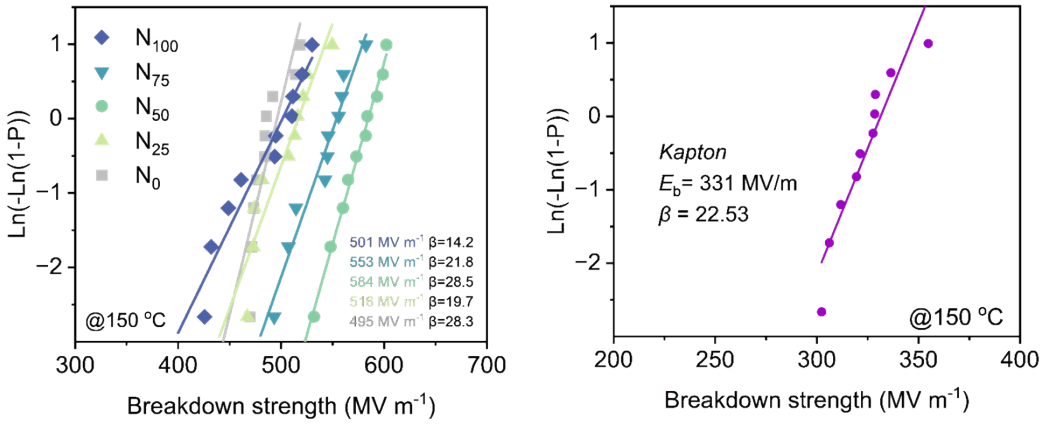

FigureS26. Two parameter Weibull distribution of dielectric breakdown field of nitrile polymers. The differences in the electric breakdown field of PIs with varying nitrile contents are not significant, primarily due to their rigid skeleton structure, the enhanced interchain charge transfer caused by polar group coupling had little effect on the breakdown electric field of these materials. Additionally, E_b of the Kapton was 331 MV m^{-1} at 150 °C, indicating the important impact of π-π interactions in PI on high-temperature breakdown performance. N_{50} exhibits the optimal breakdown strength of 584 MV m^{-1} among them, this could be attributed to the increased free volume that is advantageous in diminishing conjugation between aromatic rings, thereby suppressing the movement of charges.

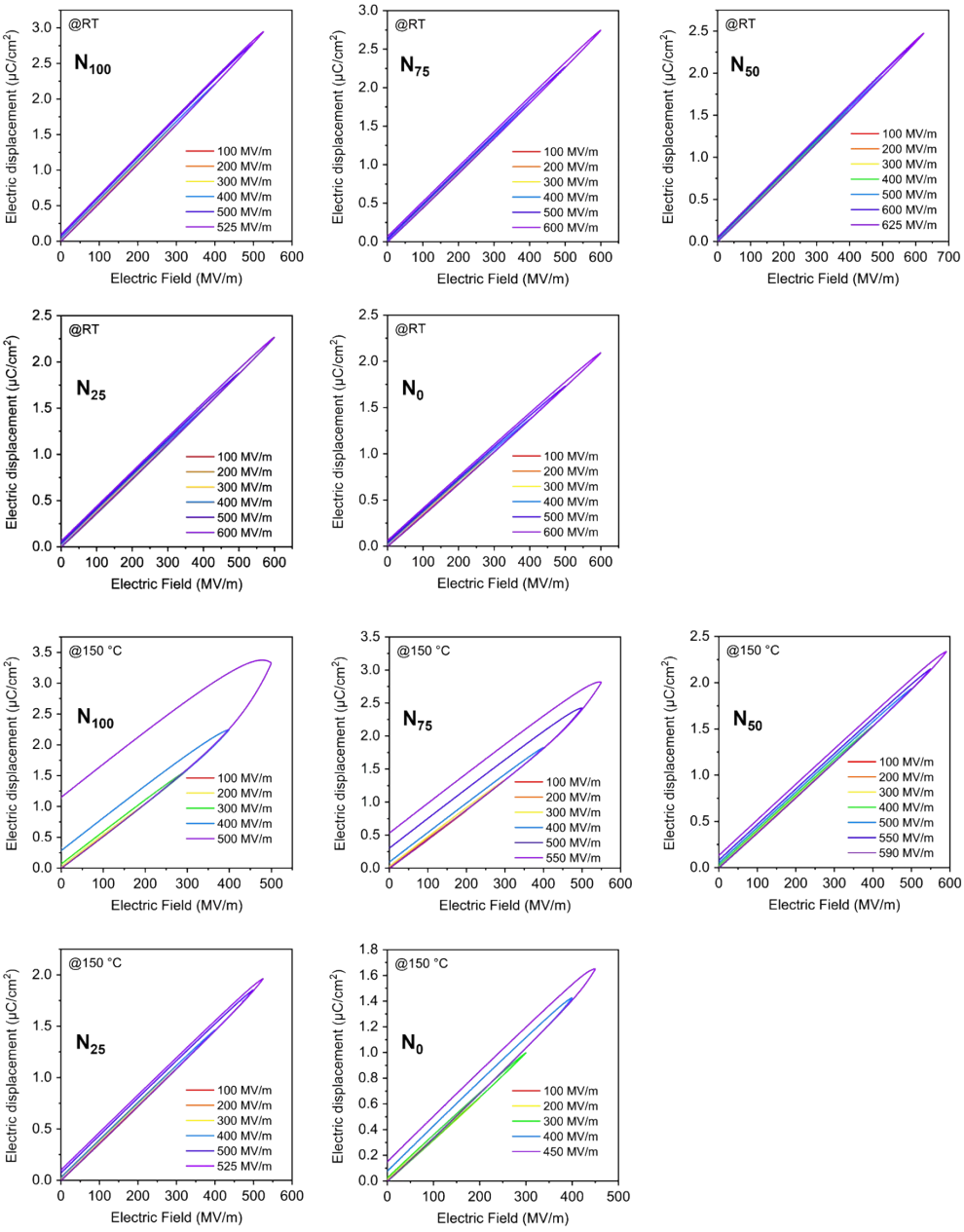

Figure S27. D-E loops of nitrile polyimides at both room temperature and 150 °C, employing a frequency of 100 Hz.

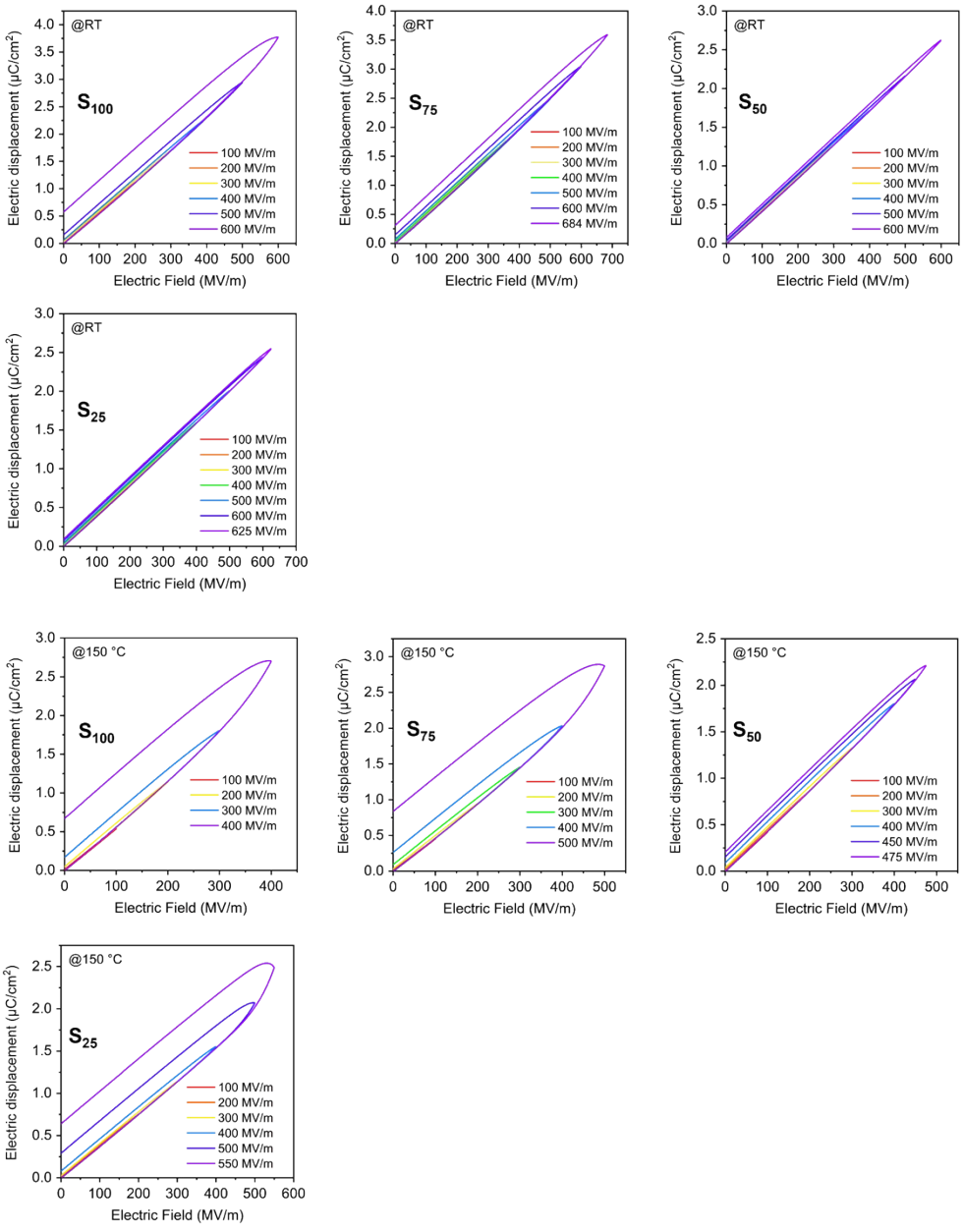

Figure S28. D-E loops of sulfone polyimides at both room temperature and 150 °C, employing a frequency of 100 Hz.

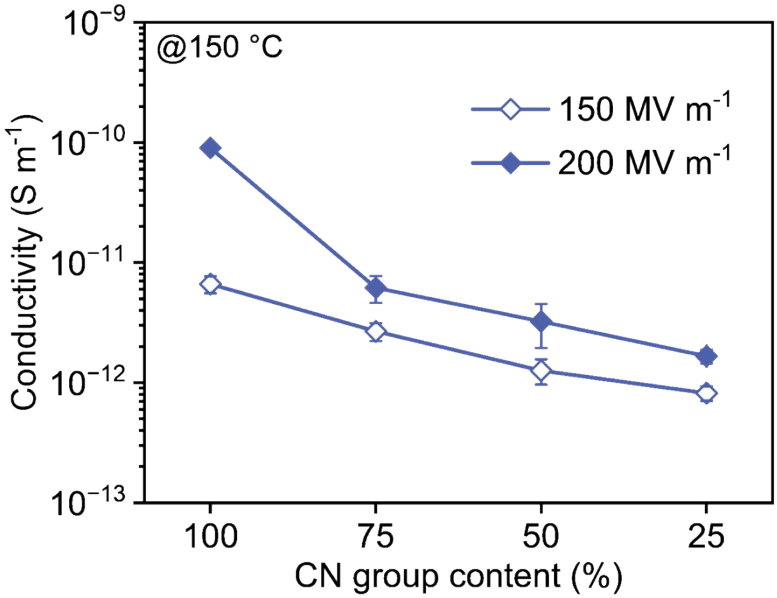

Figure S29. The conductivities of nitrile polymers, N_{100} exhibited the most significant variation in conductivity value with the increased electric field at 150 °C, from 6.6 × 10^{-12} S m^{-1} at 150 MV m^{-1} to 9.0 × 10^{-11} S m^{-1} at 200 MV m^{-1}, while the decoupled N_{50} demonstrated slightly growing conductivity from 1.2 × 10^{-12} S m^{-1} at 150 MV m^{-1} to 3.2 × 10^{-12} S m^{-1} at 200 MV m^{-1}. The conductivity loss at high temperatures can be effectively suppressed by restricting the coupling of dipoles.

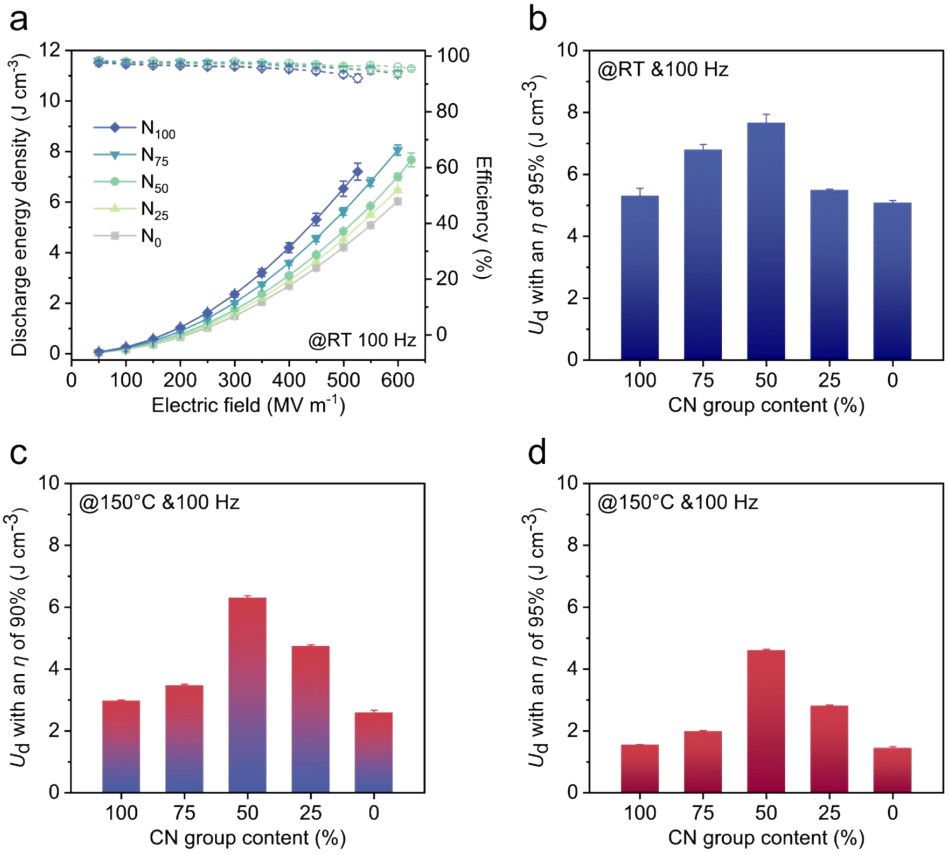

Figure S30. a) Capacitive performance of nitrile polymers at room temperature. Average discharged energy density at b) room temperature with 95% efficiency, c) 150 °C with 90% efficiency, and d) 150 °C with 95% efficiency.

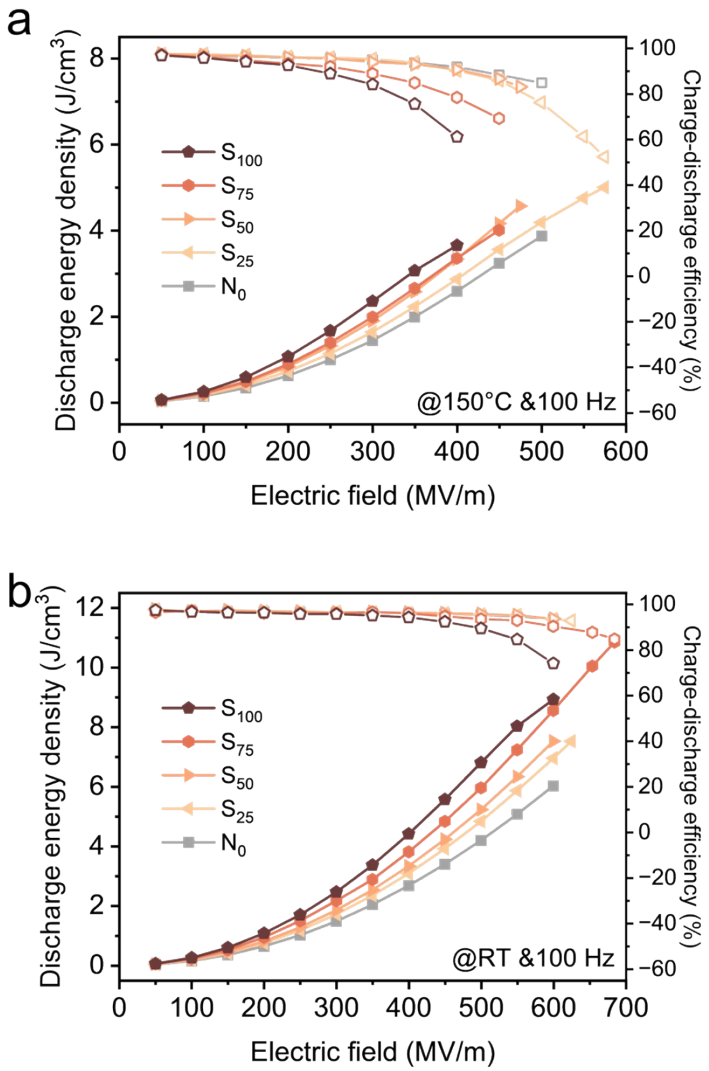

1

2 **Figure S31.** Capacitive performances. a) The energy storage properties of sulfone
3 polymers at room temperature, which all exhibit a relatively high efficiency except the
4 severe coupled S_{100}. b) The energy storage abilities of sulfone polymers at 150 °C, the
5 charge-discharge efficiencies of all sulfone polymers decreased compared with nitrile
6 polymers at high temperature and high electrical field due to the coupled dipole
7 structures.

8

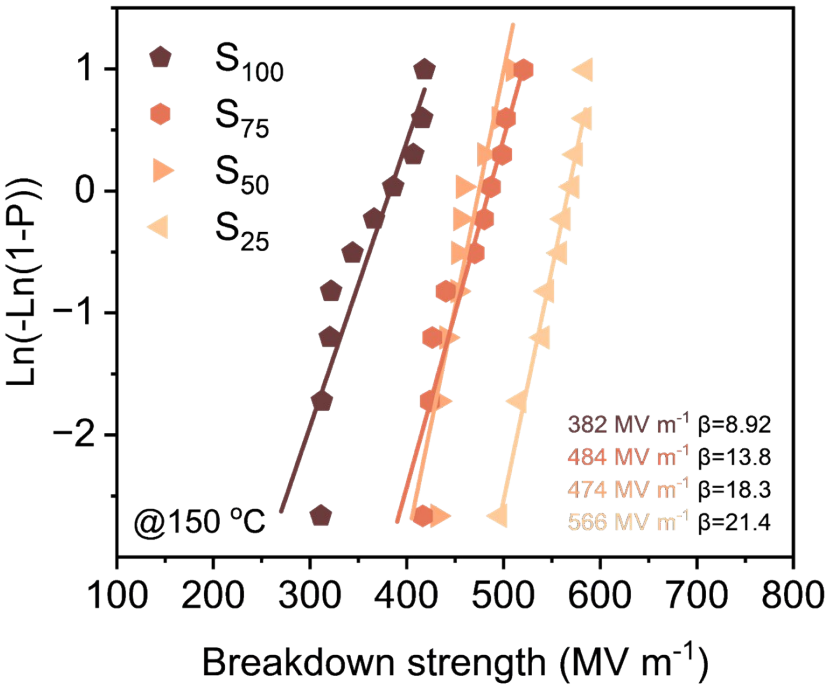

Figure S32. Dielectric breakdown fields of sulfone polymers at 150 °C, S_{100} with the most severe coupled structure shows a significantly decreased E_b.

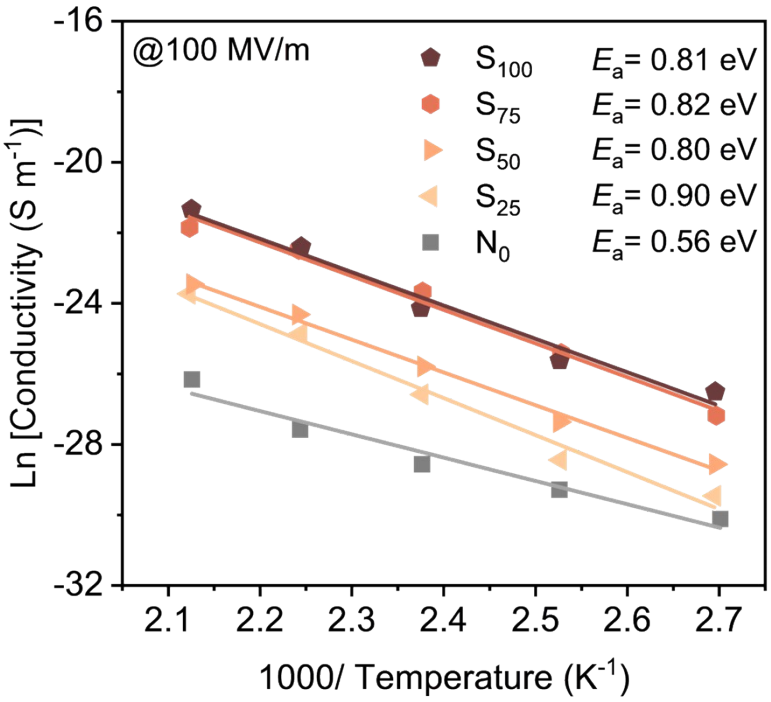

Figure S33. Temperature-dependent conductivity test. All sulfone polymers demonstrated similar activation energy, except S_{25} was a little higher than others, indicating the little difference in charge traps depth. However, their trap depths are still higher than that of N_0.

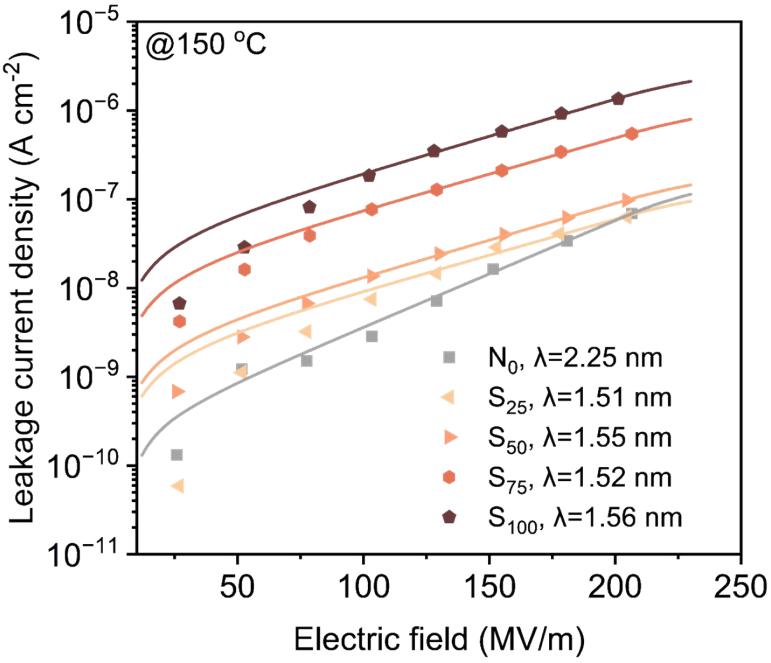

Figure S34. Hopping conduction model of sulfone polymers. Their similar hopping distance (λ) shows no significant change in their trap depths except N_0.

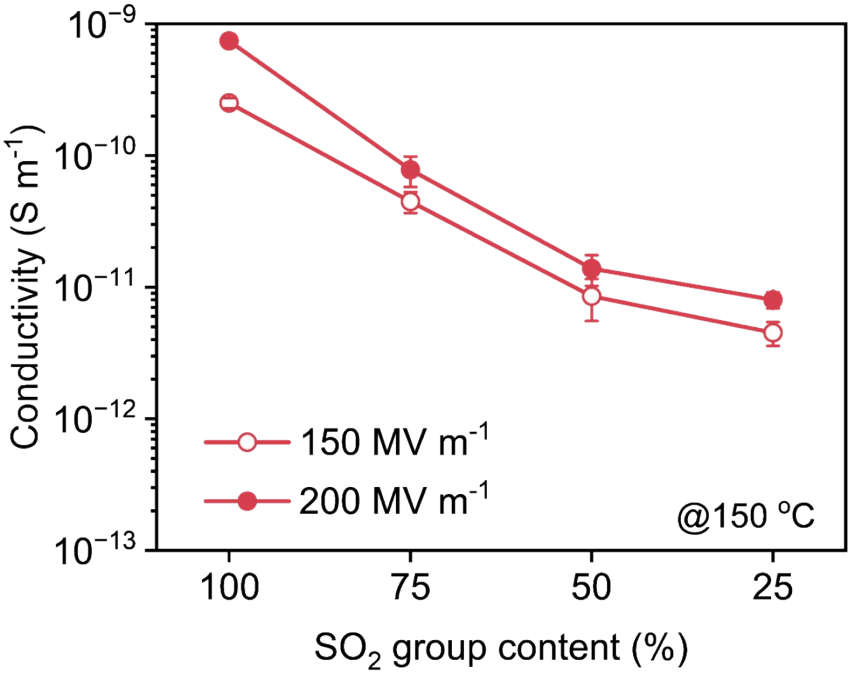

Figure S35. Conductivity of sulfone polymers under 150 °C.

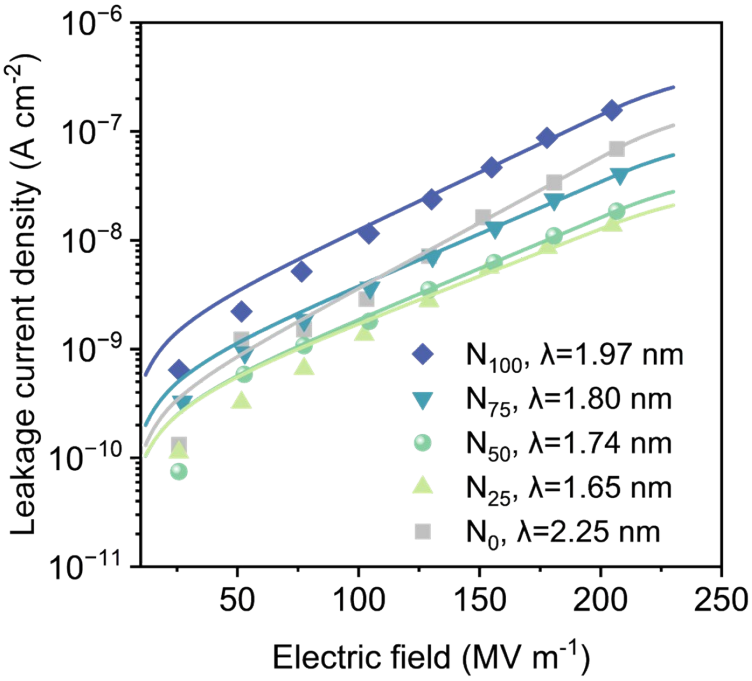

Figure S36. The hopping conduction models corroborate the charge transfer behavior exhibited by nitrile polymers, wherein distinct hopping distances, denoted as λ, progressively diminish with a decrease in nitrile content, demonstrating deeper charge traps.

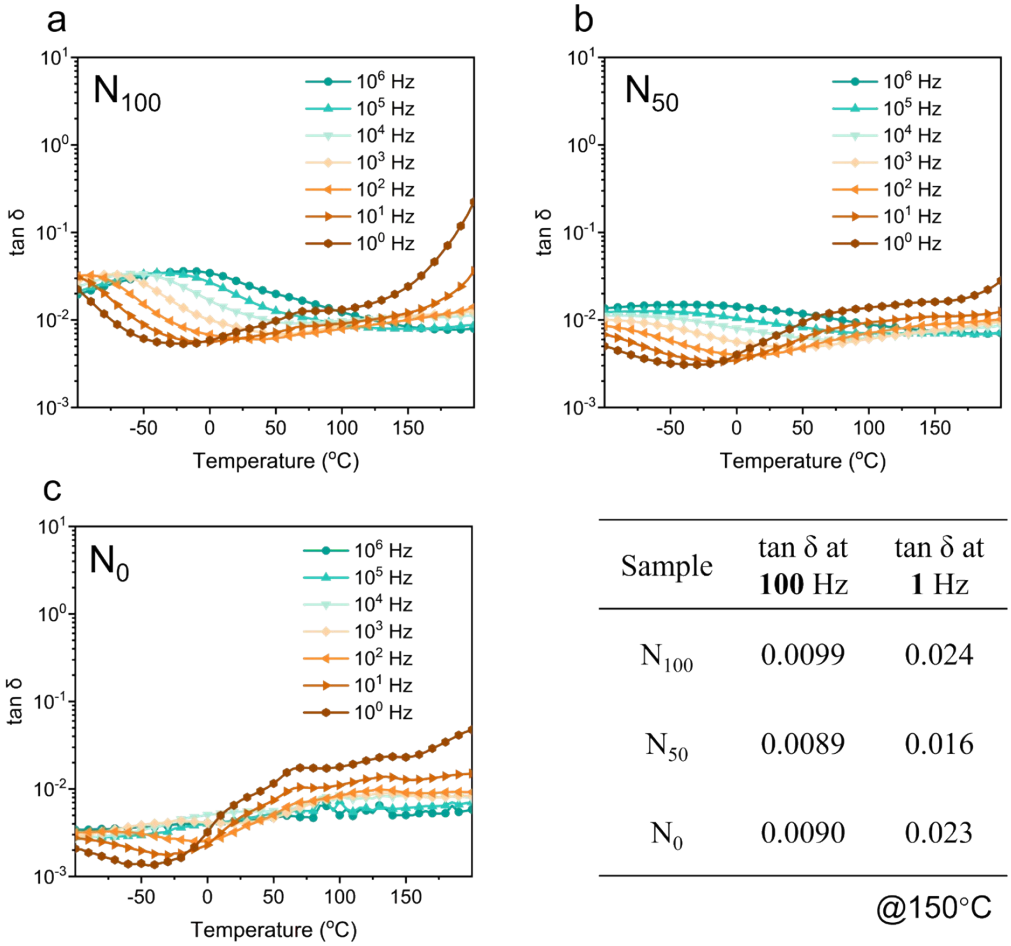

Sample	tan δ at **100** Hz	tan δ at **1** Hz
N_{100}	0.0099	0.024
N_{50}	0.0089	0.016
N_0	0.0090	0.023

@150°C

Figure S37. Temperature- and frequency- dependent tan δ of N_{100}, N_{50}, and N_0. The tan δ at low frequency (1 Hz or lower) is correlated with the conduction loss.

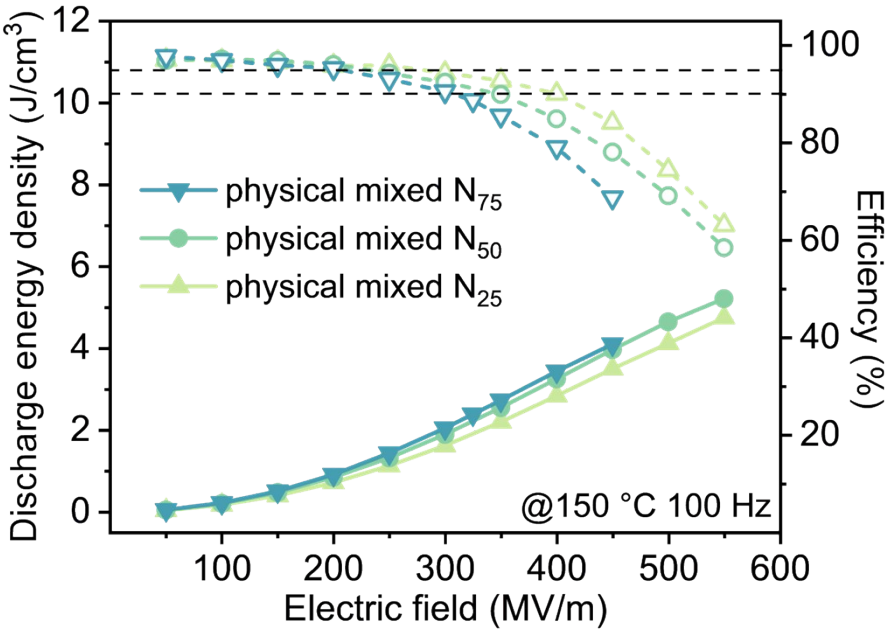

Figure S38. The energy storage abilities of physically mixed N_{75}, N_{50} and N_{25} at 150 °C, which are far worse than that of the corresponding copolymers due to the uneven distribution of dipoles. These mixtures were attained by the blend of N_{100} and N_0.

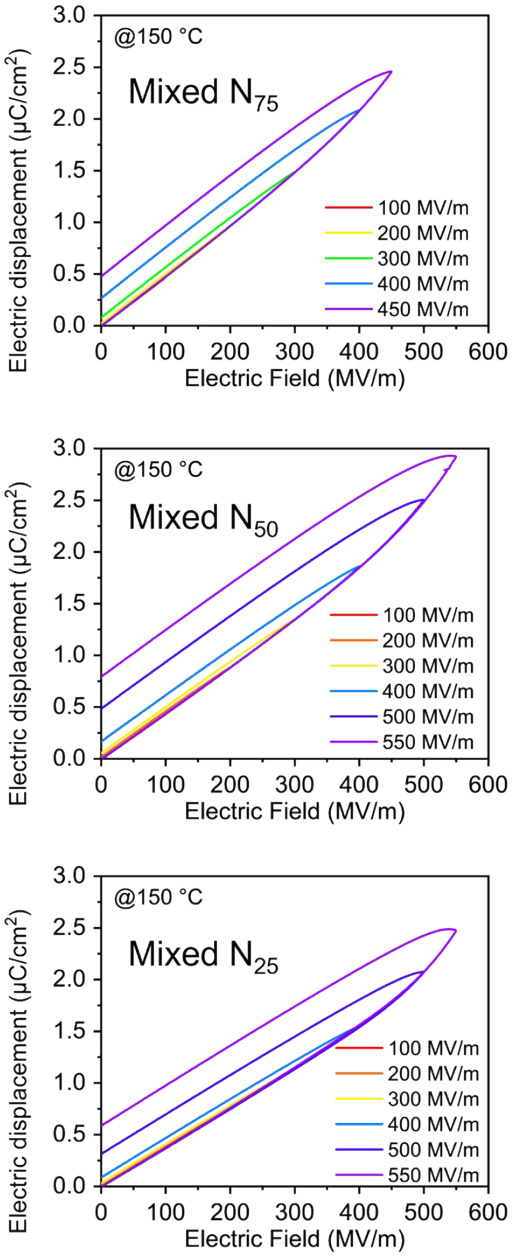

1

2 **Figure S39.** D-E loops of all physically mixed N_{75}, N_{50} and N_{25} at 150 °C & 100 Hz.

3

4

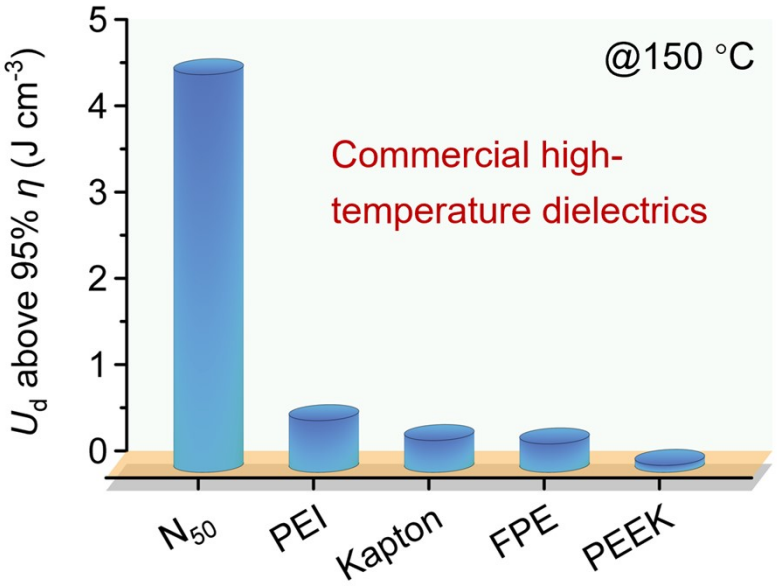

Figure S40. U_d above 95% η of N_{50} and some commercial high-temperature dielectrics. We listed several commercial high-temperature dielectric materials, such as PEEK, Kapton, FPE and PEI. In comparison, N50 demonstrated significantly superior performance at 150°C with an efficiency of 95%, along with a higher dielectric constant.

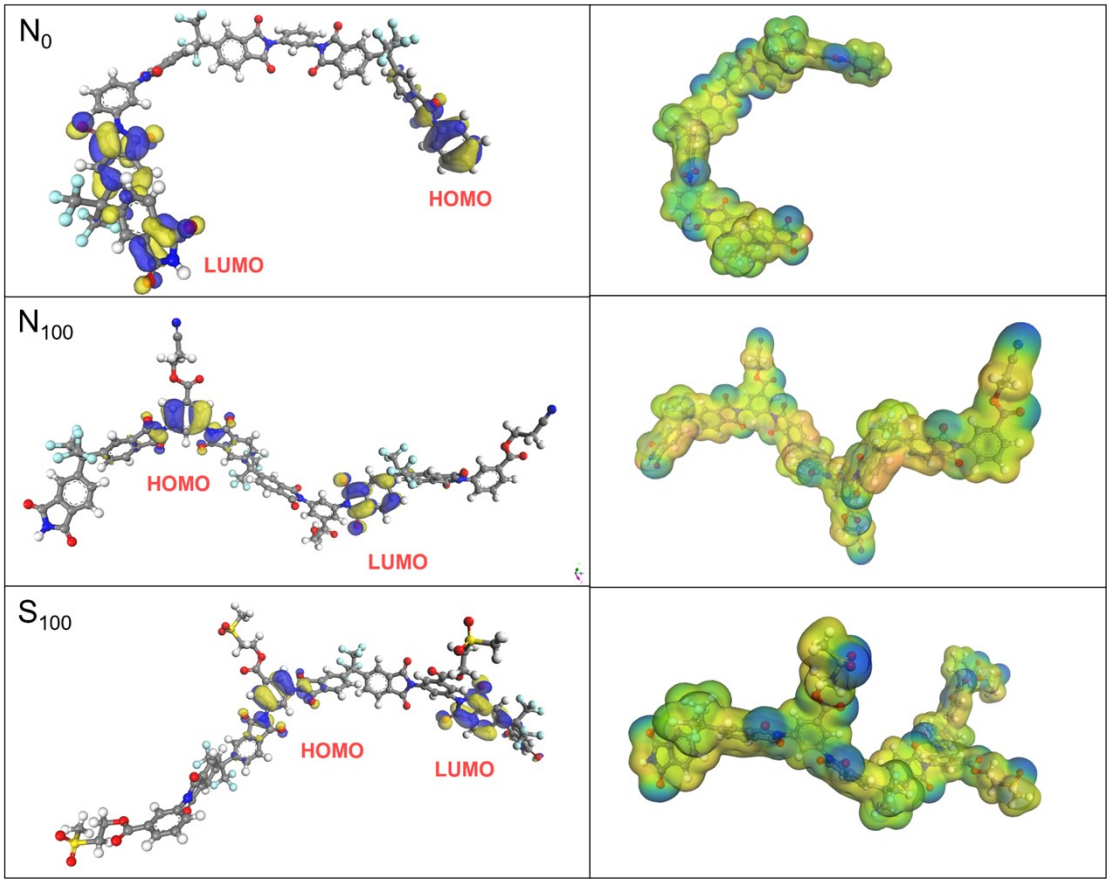

Figure S41. Orbitals and electrostatic potentials of polymers. HOMO is located at the aromatic ring connected to the polar groups in both nitrile and sulfone polymers.

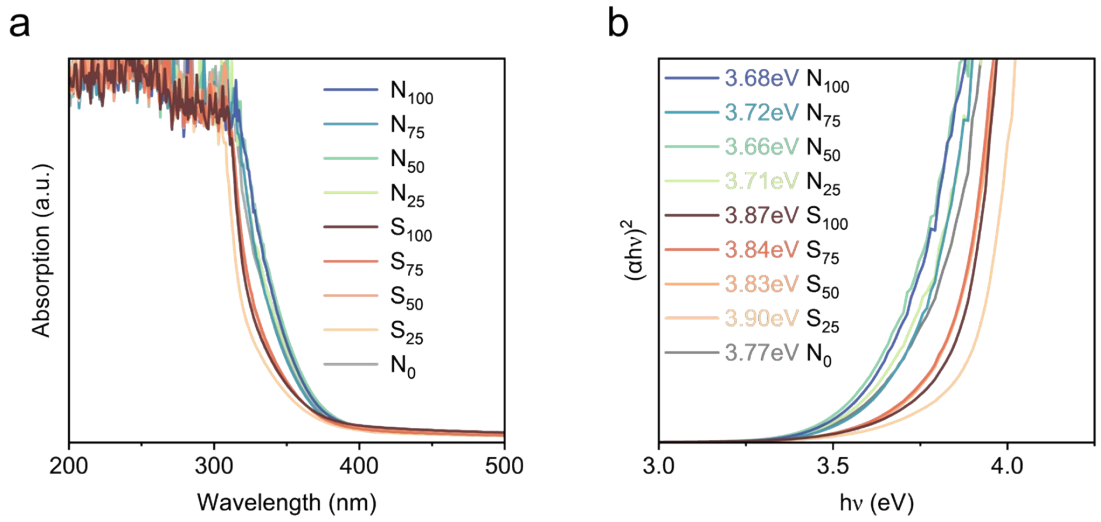

Figure S42. a) UV-vis spectra of polar polymers. b) Optical bandgaps derived from the $(\alpha h\nu)^2$-$h\nu$ plots by Tauc plot of the experimental dielectric polymers. No significant correlation between the optical bandgap and the content of polar groups.

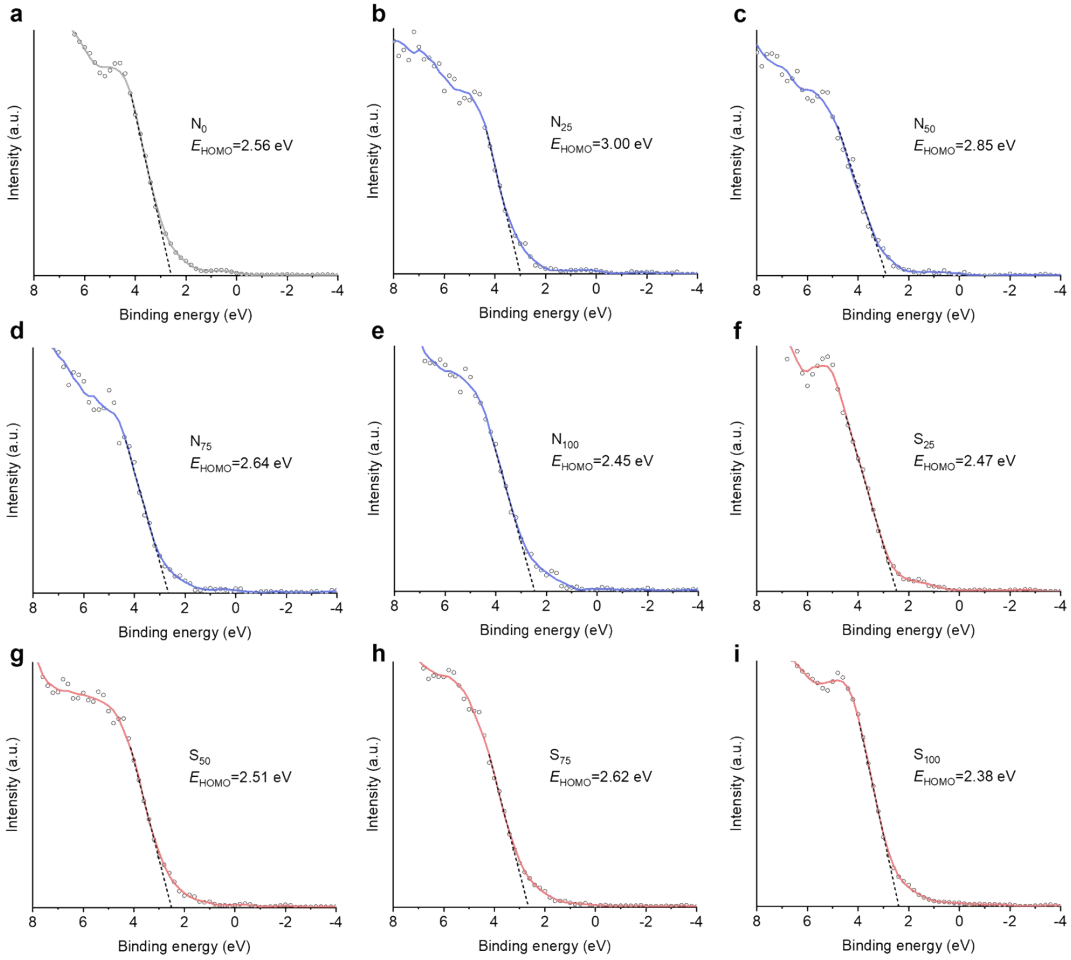

Figure S43. VB-XPS spectra of both PI-derived polymers. Where E_{HOMO} represents the energy difference between Valence band maximum and Fermi levels.

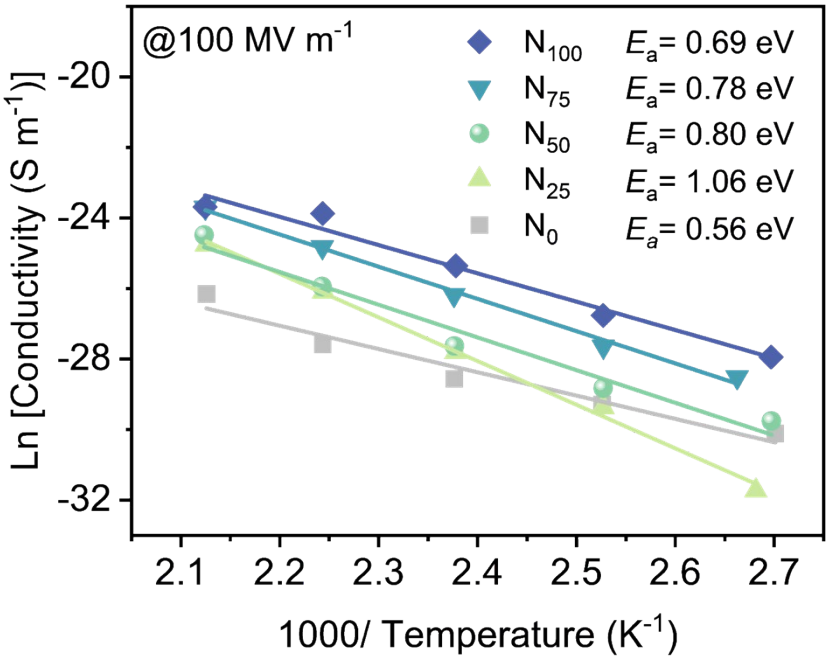

1

2 **Figure S44.** Temperature-dependent electrical conductivities of N_{100}, N_{75}, N_{50} N_{25} and

3 N_0 with the electric fields of 100 MV m^{-1} at 150 °C.

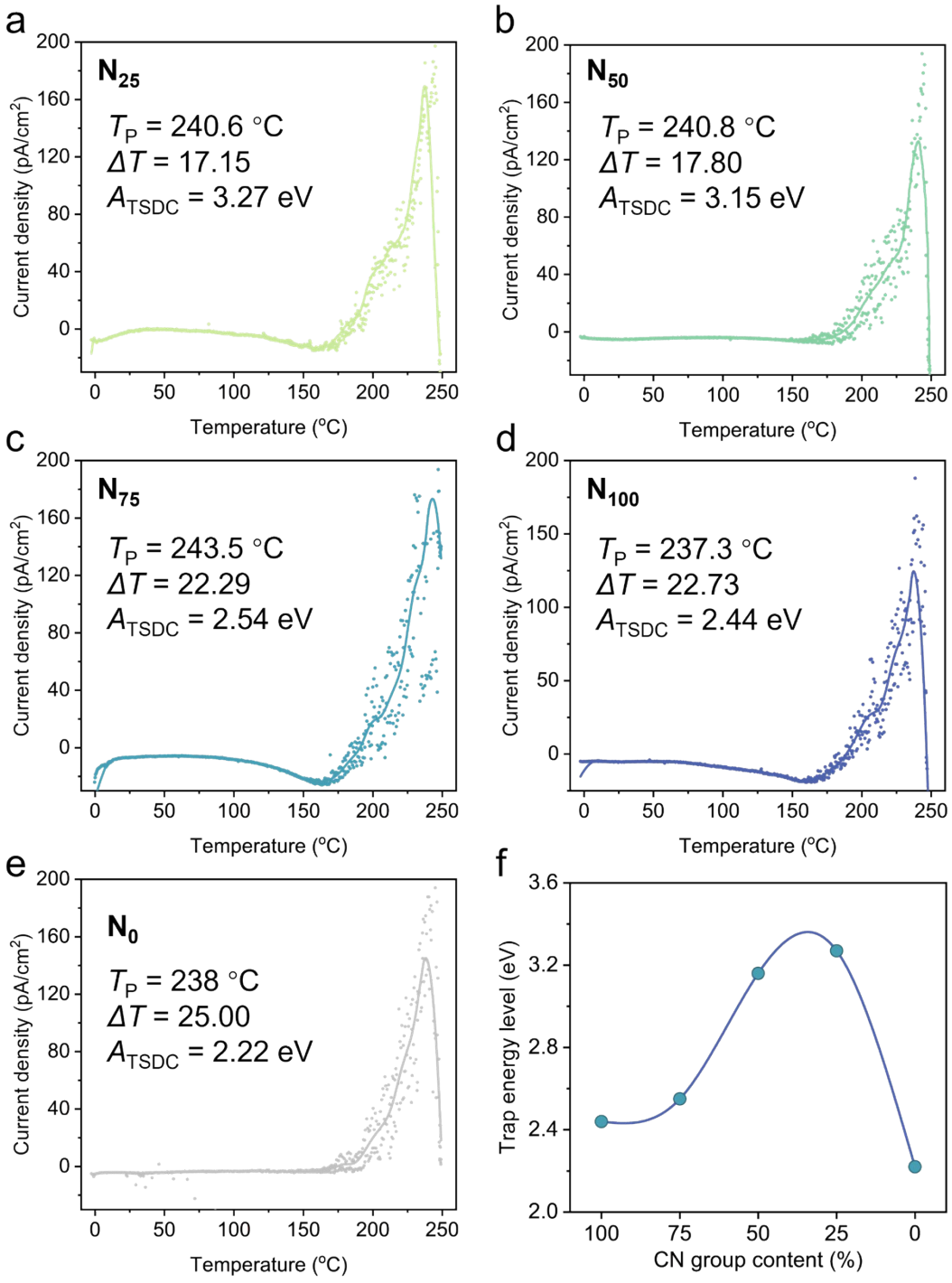

1

2 **Figure S45.** TSDC curves of nitrile polymers. Which mainly differs in their half-height

3 peak.

4

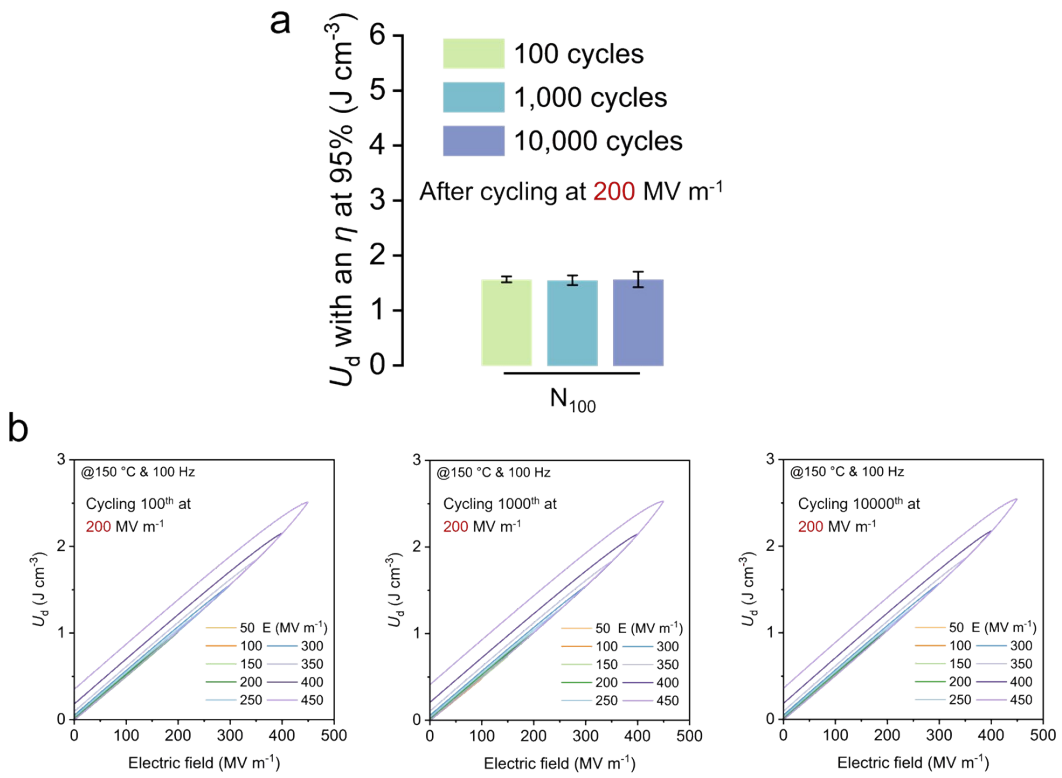

Figure S46. a) The U_d at 95% η and b) some P-E loops of N_{100} after different cycling times.

After undergoing various cycles under the electric field of 200 MV m^{-1}, the energy storage performance of N_{100} exhibited no significant changes, maintaining a discharge efficiency of approximately 95% near an electric field of 250 MV m^{-1}. Correspondingly, the U_d ranged from 1.49 to 1.64 J cm^{-3}.

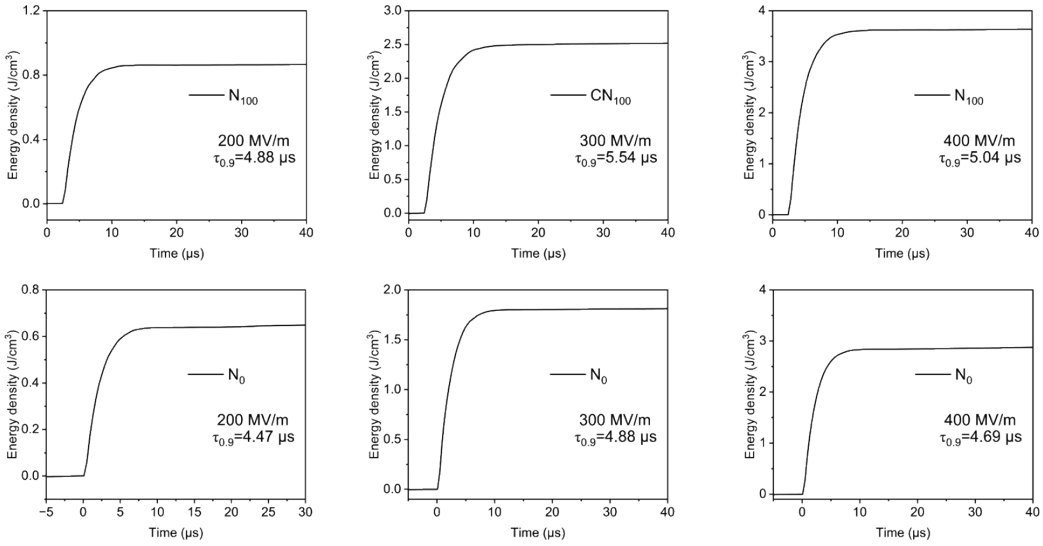

1

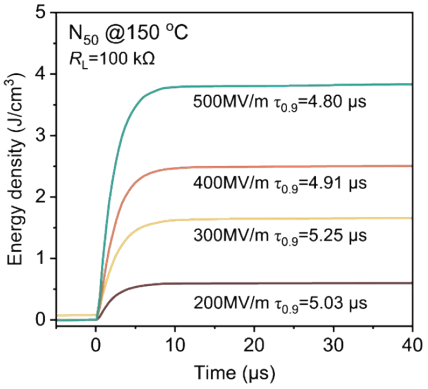

2

3 **Figure S47.** Discharge times of N_0, N_{50} and N_{100}. The rapid discharge capabilities of

4 N_{100} and N_0 are comparable to that of N_{50}, with a $\tau_{0.9}$ of approximately 5 μs.

5

6

7

8